The exploration of novel Alzheimer's therapeutic agents from the pool of FDA approved medicines using drug repositioning, enzyme inhibition and kinetic mechanism approaches

Hassan, Mubashir; Raza, Hussain; Abbasi, Muhammad Athar; Moustafa, Ahmed A.; Seo, Sung Yum

Published in:
Biomedicine and Pharmacotherapy

DOI:
10.1016/j.biopha.2018.11.115

Biomedicine & Pharmacotherapy 109 (2019) 2513–2526

Contents lists available at ScienceDirect

Biomedicine & Pharmacotherapy

journal homepage: www.elsevier.com/locate/biopha

The exploration of novel Alzheimer's therapeutic agents from the pool of FDA approved medicines using drug repositioning, enzyme inhibition and kinetic mechanism approaches

Mubashir Hassan[a, 1], Hussain Raza[a, 1], Muhammad Athar Abbasi[a,b], Ahmed A. Moustafa[c,d], Sung-Yum Seo[a,*]

[a] College of Natural Science, Department of Biological Sciences, Kongju National University, Gongju, 32588, South Korea
[b] Department of Chemistry, Government College University, Lahore, 54000, Pakistan
[c] School of Social Sciences and Psychology & MARCS Institute for Brain and Behaviour, Western Sydney University, Sydney, New South Wales, Australia
[d] Department of Social Sciences, College of Arts and Sciences, Qatar University, Doha, Qatar

ARTICLE INFO

Keywords:
Acetylcholinesterase
Drug-repositioning
Alzheimer's disease
Molecular docking
Enzyme kinetics

ABSTRACT

Novel drug development is onerous, time consuming and overpriced process with particularly low success and relatively high enfeebling rates. To overcome this burden, drug repositioning approach is being used to predict the possible therapeutic effects of FDA approved drugs in different diseases. Herein, we designed a computational and enzyme inhibitory mechanistic approach to fetch the promising drugs from the pool of FDA approved drugs against AD. The binding interaction patterns and conformations of screened drugs within active region of AChE were confirmed through molecular docking profiles. The possible associations of selected drugs with AD genes were predicted by pharmacogenomics analysis and confirmed through data mining. The stability behaviour of docked complexes (Drugs-AChE) were checked by MD simulations. The possible therapeutic potential of repositioned drugs against AChE were checked by *in vitro* analysis. Taken together, Cinitapride displayed a comparable results with standard and can be used as possible therapeutic agent in the treatment of AD.

1. Introduction

Alzheimer's disease (AD) is a neurodegenerative disorder and the utmost cause of dementia in old age [1,2]. There are more than 35 million people effected by AD every year and that number is expected to double in twenty years [3]. The etiology of AD is highly complex and yet not fully understood. However, there are some biomarkers such as low levels of acetylcholine, β-amyloid (Aβ) deposits, tau-protein aggregation, neurofibrillary tangles (NFTs), oxidative stress, and dys-homeostasis of bio-metals are used for the diagnosis of AD [4–6]. These available clinical therapeutics show only partial effectiveness in ameliorating AD symptoms and cognitive ability. Thus, designing an operative therapeutic agent to treat AD is an immediate and significant challenge in present time.

Generally, the drug development is onerous, time consuming and overpriced process with particularly low success and relatively high enfeebling rates. To aid this productivity gaps and time consuming burden, multiple computational approaches including drug repositioning are being used in recent era [7,8]. Drug repositioning approach assistances in to minimize the cost and time in drug development process due to their known efficacy and therapeutic potential against other diseases [9,10]. However, it has been observed that drug development efforts for the treatment of AD have been largely unsuccessful in the last decade. In present time, medical research emphases on the factors that are thought to contribute to AD development, such as tau proteins and Aβ deposits [11–13].

Cholinestrases are potential target for the symptomatic treatment of AD and related dementias [14–16]. Acetylcholinesterase (AChE, or acetylhydrolase) is a primary cholinesterase in the body which catalyses the breakdown of acetylcholine and some other choline esters functioning as neurotransmitters. Therefore, AChE is used as target molecule to testify the inhibitory potential of newly designed chemical structures in the treatment of AD [14]. Another research report also showed that, AChE is remained a highly viable target for the symptomatic improvement in AD because cholinergic deficit is a consistent finding in AD [17]. Donepezil (Aricept), is a centrally acting reversible

* Corresponding author.
E-mail address: dnalove@kongju.ac.kr (S.-Y. Seo).
[1] Mubashir Hassan and Hussain Raza equally contributed in the manuscript.

https://doi.org/10.1016/j.biopha.2018.11.115
Received 7 September 2018; Received in revised form 19 November 2018; Accepted 25 November 2018

AChE inhibitor used as palliative treatment against AD by increasing the level of cortical acetylcholine [18]. Donepezil exert their therapeutic action by inactivating cholinesterase which results in inhibiting the hydrolysis of acetylcholine. As a result the acetylcholine level is increased at cholinergic synapses. Donepezil has been tested in other cognitive disorders including lewy body dementia and vascular dementia, but it is not currently approved for these indications [19,20].

In current study, we proposed a computational and enzyme inhibitory mechanistic approach that aims to screen the Food and Drug Administration (FDA) approved drugs against AD. The human AChE structure having PDBID: 4EY7 (https://www.rcsb.org/structure/4ey7) was used a receptor molecule to screen FDA approve drugs. Donepezil was used as standard template to access the similar ligand structures from FDA through SwissSimilarity approach. The screened hits having similar chemical structures were accessed from FDA and undergoes docking analysis using PyRx. The best selected drugs again run into a docking procedure by Glide to check their binding affinity against AChE within active region of target protein. Moreover, pharmacogenomics analysis (drug-gene interactions) was performed by getting all possible genes against all selected drugs. Finally, enzyme inhibitory kinetic analysis was performed on best selected hits (drugs) to confirm and validate our computational prediction.

2. Methodology

2.1. Retrieval of protein structure

The protein structure of human AChE (PDBID: 4EY7) was accessed form PDB. UCSF Chimera 1.10.1 tool was employed for energy minimization by using conjugate gradient algorithm and amber force field [21]. Furthermore, VADAR 1.8 online server was used to interpret the protein architecture of helices, beta-sheets, coils and turns [22]. The Discovery Studio 2.1.0 Client was used to view 3D structure of target protein and Ramachandran graph generation [23].

2.2. Repossession of alzheimer's FDA approved drugs through shape-based screening

Donepezil is commonly known as cholinesterase inhibitor and being used in the treatment of AD as standard drug [24]. The smile format and chemical structure of donepezil was retrieved from FDA (https://www.fda.gov/). The SwissSimilarity, an online platform which allows you to identify some chemical hits from FDA and other libraries with respect to your reference structure [25]. Donepezil was used as standard template to screen FDA approved drugs. All the screened drugs were ranked according to their predicted score values. The obtained screened drugs were sketched in ACD/ChemSketch and visualized in PyMol [26].

2.3. Molecular docking using autodock VINA and glide

Before conducting our docking experiments, all the screened drugs were sketched in ACD/ChemSketch tool and accessed in mol format. Furthermore, UCSF Chimera 1.10.1 tool was employed for energy minimization of each ligand having default parameters such as steepest descent and conjugate gradient steps 100 with step size 0.02 (Å), and update interval was fixed at 10. Finally, Gasteiger charges were added using Dock Prep in ligand structures to obtain the good structure conformation. Docking experiment was performed on all screened compounds against AChE through PyRx docking tool [27]. The binding pocket of target protein (AChE) was confirmed from already published data [14]. In docking experiments, the grid box dimension values were adjusted as X = − 25.27, Y = 22.43 and Z = 0.665, respectively, with by default exhaustiveness = 8 value. We have adjusted sufficient grid box size on binding pocket residues to allow the ligands to move freely in the search space. All the screen drugs were docked separately against target protein and complexes were keenly analysed to view their binding conformational poses against target protein to obtain the best docking results. Moreover, the generated docked complexes were evaluated on the basis of lowest binding energy (kcal/mol) values and binding interaction pattern between ligands and receptor. The graphical depictions of all the docked complexes were accomplished by UCSF Chimera 1.10.1 and Discovery Studio (2.1.0), respectively.

Furthermore, another docking tool Glide was employed on best ten screen drugs against AChE. To perform a molecular docking experiment, initially protein structure was optimized using the "Protein Preparation Wizard" workflow in Schrödinger Suite [28]. Bond orders were assigned and hydrogen atoms were added to the protein. The structure was then minimized to reach the converged root mean square deviation (RMSD) of 0.30 Å with the OPLS_2005 force field. The active site of the enzyme is defined from the co-crystallized ligands from PDB and literature data [29,14]. Finally, a docking experiment was performed against best screen drugs and target protein by using Glide docking protocol [30]. The predicted binding energies (docking scores) and conformational positions of ligands within active region of protein were also performed using Glide experiment. Throughout the docking simulations, both partial flexibility and full flexibility around the active site residues are performed by Glide/SP/XP and induced fit docking (IFD) approaches [31]. The energy and binding pattern between drugs and protein was observed and their two and three dimensional graphics were saved.

2.4. Molecular dynamics (MD) simulations

Top ten screened drugs-complexes having good energy values were selected to understand the residual backbone flexibility of protein structure; MD simulations were carried out by Groningen Machine for Chemicals Simulations (GROMACS 4.5.4 package [32]), with GROMOS 96 force field [33]. The overall system charge was neutralized by adding ions. The steepest descent approach (1000 ps) for protein structure was applied for energy minimization. For energy minimization the nsteps = 50,000 were adjusted with energy step size (emstep) 0.01 value. Particle Mesh Ewald (PME) method was employed for energy calculation and for electrostatic and van der waals interactions; cut-off distance for the short-range VdW (rvdw) was set to 14 Å, whereas neighbour list (rlist) and nstlist values were adjusted as 1.0 and 10, respectively, in em.mdp file [34]. This method permits the use of the Ewald summation at a computational cost comparable with that of a simple truncation method of 10 Å or less, and the linear constraint solver (LINCS) [35] algorithm was used for covalent bond constraints and the time step was set to 0.002 ps. Finally, the molecular dynamics simulation was carried out at 100 ns with nsteps 50,000,000 in md.mdp file. Different structural evaluations such as root mean square deviations and fluctuations (RMSD/RMSF), solvent accessible surface areas (SASA) and radii of gyration (Rg) of back bone residues were analysed through Xmgrace software (http://plasma-gate.weizmann.ac.il/Grace/) and UCSF Chimera 1.10.1 software.

2.5. Designing of pharmacogenomics networks

To design the pharmacogenomics network model for best selected drugs, Drug Gene Interaction Databases (DGIdb) [36] and Drug Signatures Database (DSigDB) [37] were employed to obtain the possible list of different disease associated genes. Furthermore, a detail literature survey was performed for each gene to identify its involvement in AD. The clumps of different diseases associated genes were sorted on the basis of AD and remaining disease associated genes were eliminated from the dataset. Finally, cystoscope an open source software for visualizing molecular interaction networks were used to build and to analyse the interaction pattern between drug and genes [38].

2.6. AChE inhibition assay

The best screened drugs (Cinitapride, Risperidone, Domperidone, Tamsulosin and Verapamil) of analytical grade were taken from Pacific Pharmaceuticals Ltd, Lahore, Pakistan to check the inhibition activity against AChE. The inhibitory activities of selected drugs were determined spectrophotometrically using acetylthiocholine iodide as substrate by following the reported methods with some modifications [39–41]. Briefly, The assay solution consisted of 180 µL of 50 mM Tris HCl buffer, pH 7.7, containing (0.1 M sodium chloride and 0.02 M magnesium chloride) and 20 µL of enzyme (AChE, EC 3.1.1.7, (from human erythrocytes) solution (0.03 U/mL); increasing concentrations of test inhibitor (10 µL) were added to the assay solution and pre incubated for 30 min at 4 °C. After that 5,5′Dithiobis (2-nitrobenzoic acid) (0.3 mM, 20 µL) and acetylthiocholine iodide (1.8 mM, 20 µL) were added to the reaction mixture and incubated at 37 °C for 10 min, followed by the measurement of absorbance at 412 nm. For non-enzymatic reaction, the assays were carried out with a blank containing all components except acetylcholinesterase. The assay measurements were measured at 412 nm using a micro plate reader (OPTI Max, Tunable). Wave-length range 340–850 nm; for 96well plates). The reaction rates were compared and the percent inhibition due to the presence of tested inhibitors was calculated. Neostigmine methylsulfate and donepezil were used as reference inhibitors. Each concentration was analysed in three independent experiments run in triplicate. IC_{50} values were calculated by nonlinear regression using GraphPad Prism 5.0.

The % of Inhibition of AChE was calculated as following

$$\text{Inhibition (\%)} = [(\text{B-S})/\text{B}] \times 100$$

Here, the B and S are the absorbances for the blank and samples, respectively.

2.7. Determination of AChE inhibition kinetics

On the basis of IC_{50}, we select the most potent Cinitapride for kinetic analysis. A series of experiments were performed to determine the inhibition kinetics of Cinitapride by following the already reported method [14]. Kinetics were carried out by varying the concentration of acetylthiocholine iodide the presence of different concentrations of Cinitapride (0.00, 0.0586, 0.1172 and 0.2344 µM). Briefly the acetylthiocholine iodide concentration was changed from 4, 2, 1, 0.5, 0.25 and 0.125 mM for acetylthiocholine iodide kinetics studies and remaining procedure was same for all kinetic studies as describes in AChE inhibition assay protocol. Maximal initial velocities were determined from initial linear portion of absorbances up to 5 min after addition of enzyme at every 30 s interval. The inhibition type on the enzyme was assayed by Lineweaver-Burk plot of inverse of velocities (1/V) versus inverse of substrate concentration 1/[S] mM^{-1}. The EI dissociation constant K*i* was determined by secondary plot of 1/V versus inhibitor concentration. The results (change in absorbance per sec) were processed by using SoftMaxPro software.

3. Results and discussion

The overall research flow sheet diagram which depicted the basic hierarchy of our newly designed work (Fig. 1).

3.1. AChE structural assessment

Human AChE is a hydrolase protein having single chain and comprises 543 residues. The VADAR 1.8 structure analysis of human AChE depicted that, it consists of 33% α-helices, 24% β-sheets, 41% coils and 21% turns. The general structure of AChE is mentioned in supplementary data (Figure. S1). The Ramachandran plots and values indicated that 93.50% of amino acids were existed in favoured region. The Ramachandran graph values showed a good accuracy of phi (φ) and psi (ψ) angles among the coordinates of receptor and most of residues were plunged in acceptable region. The Ramachandran and hydrophobicity graphs are mentioned in supplementary data (Figure. S2).

3.2. Shape based screening and retrieval of similar drugs

In drug repositioning approach, the shape-based screening, molecular docking and drug-genes association are significant parameters to predict the possible therapeutic effects of known drugs against different targets [42,43]. Our SwissSimilarity results showed that 36 drugs were selected from 1516 FDA approved drugs which showed approximately good structural resemblance with standard drug (Fig. 2). The screened drugs were ranked on the basis of similarity scoring values, ranged for 0-1. The 0 value represents dissimilarity between compounds whereas, 1 is used for highly identical compounds in screening approach. In our results the scoring values for all screen drugs is range from 0.006-0.184 as tabulated in Table 1. Although SwissSimilarity scoring values were low relative to the reference standard value range, therefore, a detail docking study was run against all screened 36 drugs to check their binding interactions behaviour in comparison with donepezil. Based on these docking results drugs were selected for further analysis.

3.3. Molecular docking using PyRx

Molecular docking experiment is best approach to study the binding conformation of ligands within the active region of target proteins [44–47]. To evaluate the best drug, all the screened drugs were docked against AChE separately and complexes were analysed on the basis of the lowest binding energy values (kcal/mol). Table 2 results showed that most of drugs exhibited comparable energy value compared to donepezil docking energy value. Darifenacin showed lowest energy value (-13.1 kcal/mol) compared to all other screened drugs. Similarly, Bosutinib, Crizotinib, Dienogest and Domperidone, also displayed good docking energy values (-12.3,-11.6, -11.2, -10.8 kca/mol), respectively. Fluspirilene and risperidone both exhibited -11.10 kcal/mol while few other drugs also possessed lower than standard energy values such as Sertindole and Tetrabenazine -9.60 and -8.90 kcal/mol. To better compare our docking results donepezil was docked against AChE having same parameters and observed that it possessed -10.7 kcal/mol. The docking energy calculation for all docking complexes was evaluated by using Eq. (1).

$$\Delta G\text{binding} = \Delta G\text{gauss} + \Delta G\text{repulsion} + \Delta G\text{hbond} + \Delta G\text{hydrophobic} + \Delta G\text{tors}\ldots \quad (1)$$

Here, ΔGgauss: attractive term for dispersion of two gaussian functions, ΔGrepulsion: square of the distance if closer than a threshold value, ΔGhbond: ramp function also used for interactions with metal ions, ΔGhydrophobic: ramp function, ΔGtors: proportional to the number of rotatable bonds.

Based on docking energy values results, ten drugs (Fluspirilene, Tamulosin Domperidone, Risperidone, Cinitapride, Bosutinib, Verapamil, Tetrabenazine, Sertindole and Darifenacin) showed comparable results with donepezil docking energy value and selected for further analyses. The standard error for Autodock is reported as 2.5 kcal/mol (http://autodock.scripps.edu/). Present docking results justified that the energy value difference among all docking complexes were comparable with standard error value.

3.4. Binding pocket analysis of AChE

The AChE binding pocket identification was confirmed by protein crystal data form PDB (4EY7) as well as from data mining [14]. This co-crystal structure was used because the donepezil was bound within active region of target protein which helps in identification of binding

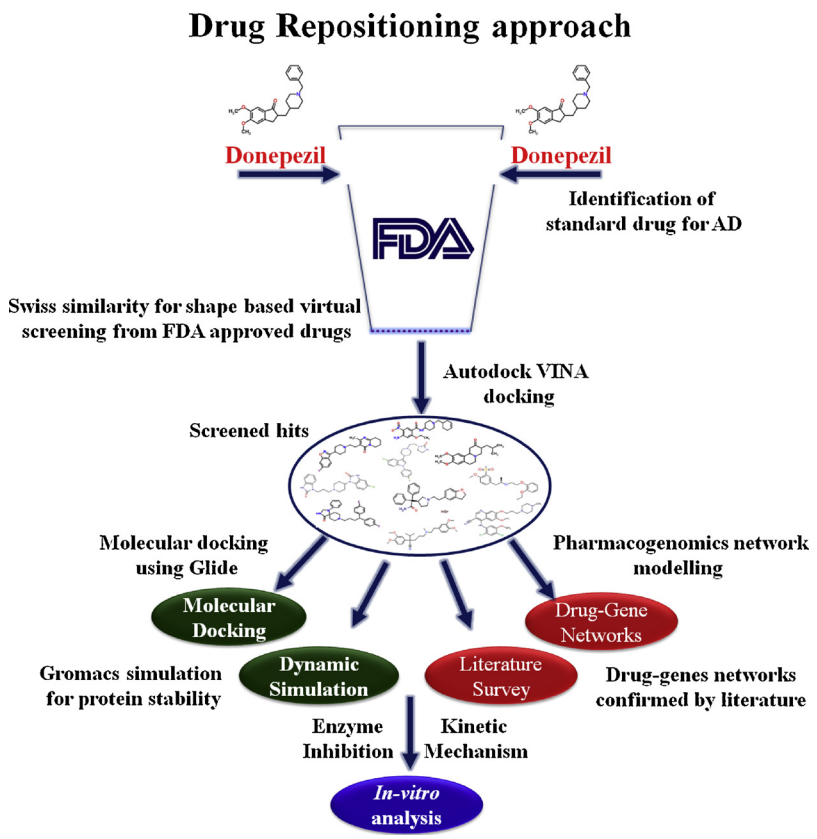

Fig. 1. The flowsheet diagram of our designed work.

pocket residues. Moreover, significant ligand conformation with respect to its target molecule helps in comparisons with our selected ligands by superimposition. The active site of this enzyme is buried inside a narrow gorge of 20 Å deep, which permits multiple enzyme-substrate interaction thereby facilitating the formation of the transition state of ACh [48,49,29]. The binding sites are often a significant constituents of the functional characterization of enzymes. Moreover, in molecular docking, the binding of ligands within the active site of target protein can predict good results compared to binding of other protein sites. Fig. 3 showed the binding pocket and targeted residues involved in Donepezil binding interaction. Here seven residues such as Trp286, Tyr72, Tyr124, Tyr341, Phe338, Tyr337, Glu202 and Trp86 are probably the counterpart of binding site. The drugs having potential to binds within this active region and interact with these residues may consider as a good candidate against AChE.

3.5. Glide docking analysis on screened drugs

Based on Swisssimilarity and PyRx VINA docking results, the 10 drugs (Fluspirilene, Tamulosin Domperidone, Risperidone, Cinitapride, Bosutinib, Verapamil, Tetrabenazine, Sertindole and Darifenacin) were selected and further undergone docking analysis using Glide (Schrodinger Suite) to exactly check the binding configurations of each drug within the active region of the AChE. The docking energy values sowed that Tamulosin showed much better docking energy results (-8.22 kcal/mol) compared to other drugs. Fluspirilene was at lowest range having energy value -2.96 kcal/mol. The other drugs such as Domperidone, Risperidone Cinitapride, Bosutinib, Verapamil, Tetrabenazine, Sertindole and Darifenacin showed hierarchal energy values -7.24, -7.04, -6.87, -6.41, -5.72, -5.60, -5.39 and -5.37 kcal/mol, respectively (Fig. 4A). Glide uses couple of scoring functions Emodel [50] and GlideScore [51] which are involved in the selection of protein-ligand complexes and ranked the ligands as per scoring values respectively. GlideScore is also based on ChemScore (fitness function), but includes a steric-clash term, adds buried polar terms devised by Schrödinger to penalize electrostatic mismatches. The GScore is calculated as from the Eq. (2).

$$\text{GScore} = \text{vdW} + \text{Coul} + \text{Lipo} + \text{Hbond} + \text{Metal} + \text{BuryP} + \text{RotB} + \text{Site}\ldots \quad (2)$$

vdW = Van der Waals energy, Coul = Coulomb energy, Lipo = Lipophilic, Hbond = Hydrogen-bonding, Metal = Metal-binding, BuryP = Penalty for buried polar groups, RotB = Penalty for freezing rotatable bonds and Site = Polar interactions in the active site.

3.6. Superimposition of screened drugs within active region of AChE

All the docked structures were superimposed to check the binding configurations of all drugs within the active region of AChE. The binding pocket analysis showed that all the screened drugs were narrowed in the binding pocket and bind with similar residues having different conformational poses within binding pocket of AChE. The binding of all drugs at the same position also justified the docking reliability and predicted results (Fig. 4 A,B).

3.7. Tamsulosin and domperidone binding analysis

The docked complexes of both Tamsulosin and Domperidone were analysed on the basis of interactions pattern of binding pocket residues. The Tamsulosin binds with AChE in good conformational position inside active region encompassed by Trp286, Tyr72, Asp74, Leu76, Tyr124, Gly121, Gly120, Tyr133, Glu202, Ser203, Ile4511, Trp86, Gly448, His447, Tyr337, Phe338, Tyr341, Gly342, Phe297, Phe295, Val294 and Ser293 residues. The 2-methoxy-phenoxy part of Tamsulosin showed its presence within the bottom side of binding pocket and binds with Trp86 via π-π staking interaction. 2-methoxy-

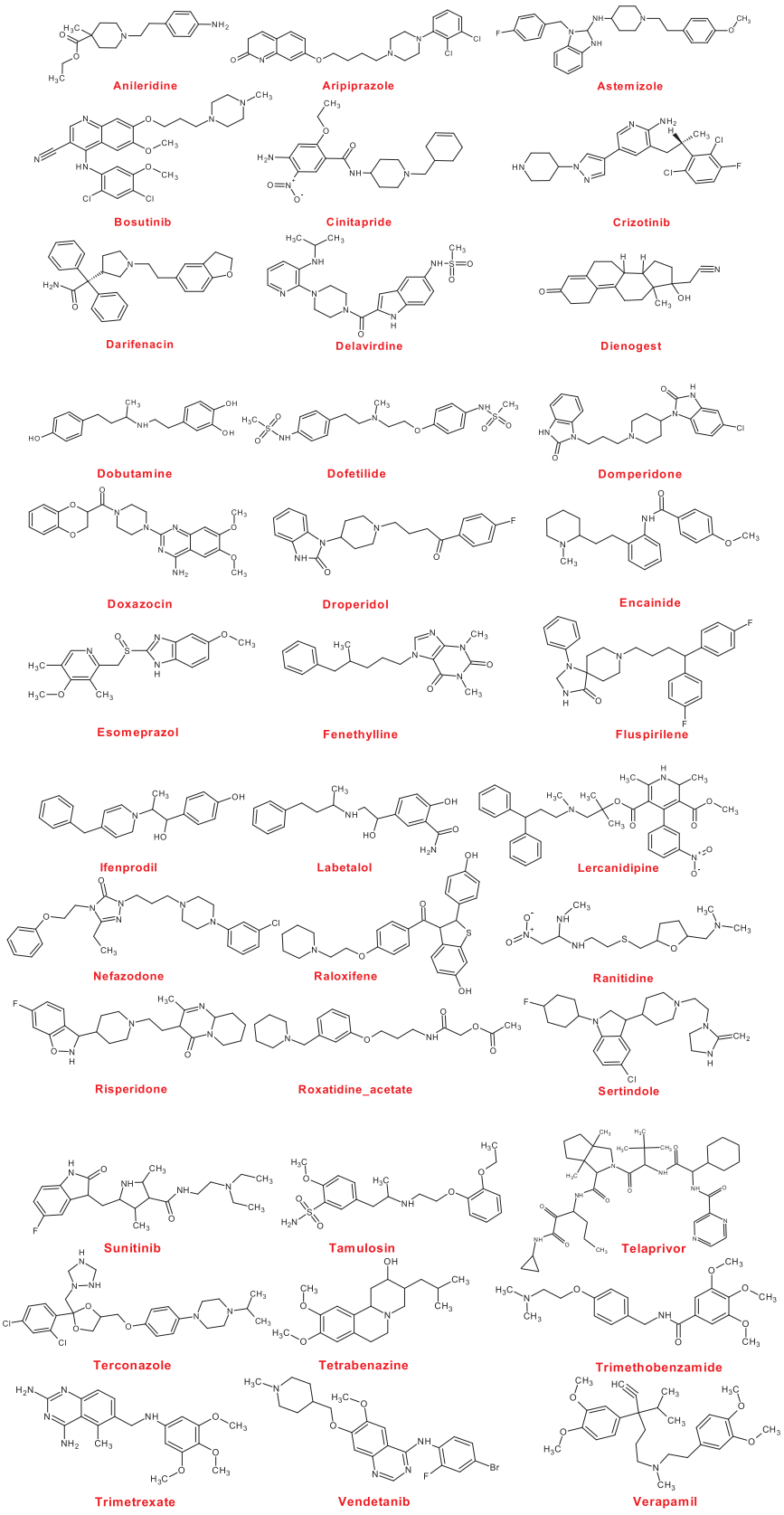

Fig. 2. Screened drugs with 2D graphical depiction.

benzene sulphonamide structure of Tamsulosin binds in the opening region of binding pocket against target protein. The crystal and published data reports showed that Trp86 is present in the binding pocket of AChE and shows its attachment with donepezil and other inhibitors [52]. The Domperidone docking complex showed that couple of hydrophobic interactions were observed against Trp286 and Tyr337,

Table 1
SwissSimilarity scoring values of screened drugs.

Drugbank IDs	Screened Drugs	Score	Drugbank IDs	Screened Drugs	Score
DB00913	Anileridine	0.008	DB08954	Ifenprodil	0.006
DB01238	Aripiprazole	0.013	DB00598	Labetalol	0.007
DB00637	Astemizole	0.011	DB00528	Lercanidipine	0.013
DB06616	Bosutinib	0.012	DB01149	Nefazodone	0.010
DB08810	Cinitapride	0.023	DB00481	Raloxifene	0.012
DB08865	Crizotinib	0.010	DB00863	Ranitidine	0.009
DB00496	Darifenacin	0.012	DB00734	Risperidone	0.010
DB00705	Delavirdine	0.007	DB08806	Roxatidine_acetate	0.016
DB08866	Dienogest	0.009	DB06144	Sertindole	0.024
DB00841	Dobutamine	0.006	DB01268	Sunitinib	0.011
DB00204	Dofetilide	0.009	DB00706	Tamsulosin	0.021
DB01184	Domperidone	0.012	DB05521	Telaprevir	0.008
DB00590	Doxazosin	0.007	DB00251	Terconazole	0.007
DB00450	Droperidol	0.010	DB04844	Tetrabenazine	0.184
DB01228	Encainide	0.007	DB00662	Trimethobenzamide	0.012
DB00736	Esomeprazole	0.006	DB01157	Trimetrexate	0.012
DB01482	Fenethylline	0.008	DB05294	Vandetanib	0.011
DB04842	Fluspirilene	0.011	DB00661	Verapamil	0.015

Table 2
Docking energy values of donepezil against AChE.

AChE docked complexes	Binding Affinity (kcal/mol)	AChE docked complexes	Binding Affinity (kcal/mol)
Anileridine.	−10	Labetalol	−9.8
Aripiprazole	−9.1	Lercanidipine	−10.2
Astemizole	−8.9	Nefazodone	−9.8
Bosutinib	−12.3	Raloxifene	−9.3
Cinitapride	−8.3	Ranitidine	−7
Crizotinib	−11.6	Risperidone	−11.1
Darifenacin	−13.1	Roxatidine_acetate	−8.9
Dobutamine	−7.8	Sertindole	−9.6
Dofetilide	−7.9	Sunitinib	−8.7
Dienogest	−11.2	Tamsulosin	−10.8
Domperidone	−10.8	Telaprevir	−10.6
Doxazosin	−9.1	Terconazole	−8.7
Droperidol	−8.1	Tetrabenazine	−8.9
Encainide	−8.1	Trimethobenzamide	−8.4
Esomeprazole	−9.7	Trimetrexate.	−8.4
Fenethylline	−8.6	Trimetrexate	−8.4
Fluspirilene	−11.1	Vandetanib	−9.5
Ifenprodil	−8.2	Verapamil	−10.5

respectively. In Domperidone structure, two benzimidazol-2-one groups are attached at outside of drug. The attachment of choloro group with benzimidazol-2-one cause hindrance to properly enter inside the binding pocket of AChE. However, benzimidazol-2-one with any moiety showed their entrance inside the binding pocket of target protein and showed their binding with Tyr337. While in the opening region of target protein 5-chloro-benzimidazol-2-one forms bond with Trp286. The surrounded residues are Phe297, Phe295, Val294, Gly448, His447, Tyr124, Phe338, Val340, Tyr341, Tyr72, Asp74 and Leu76. Existing data also ensured the importance of these residues in bonding with other AChE inhibitors which strengthen our docking results [53]. The graphical depiction of both docking complexes are mentioned in Fig. 5 and their 2D depiction in supplementary data Figure. S3.

3.8. Risperidone and cinitapride binding analysis

The docked complexes of both risperidone and cinitapride were examined on the basis of interaction behaviour within active binding site residues of AChE. Risperidone binds with AChE in good conformational position inside active region. In risperidone docking, three bonds were observed against Tyr72, Phe295 and Tyr341, respectively. The nitrogen atom of primidone form good interaction with Tyr72 whereas, oxygen atom of benzoxazole ring form interaction with Phe295. Another, π-π staking interaction was observed between benzene ring of Tyr341 and benzoxazole. The existing data showed good correlation with the interacted residues which strengthen our docking results (Lu et al., 2011). The other binding pocket residues present

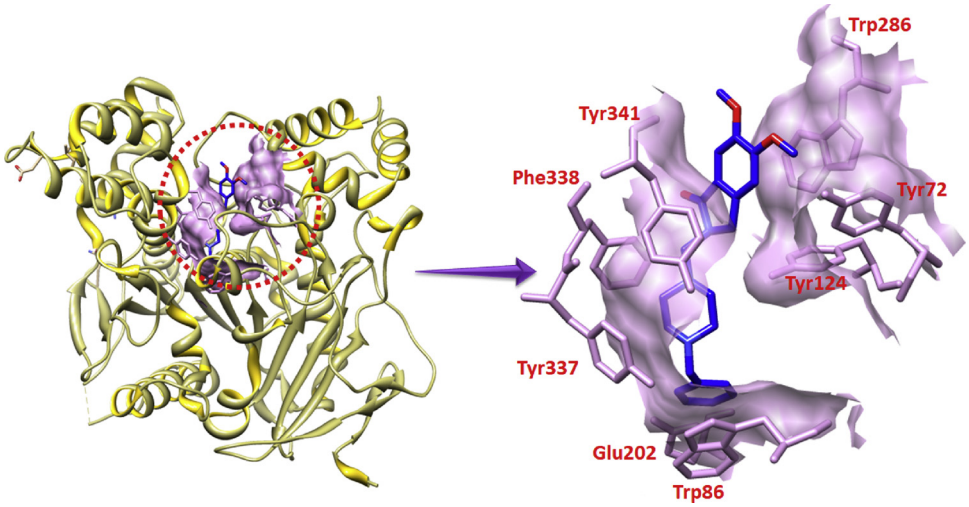

Fig. 3. Binding pocket of AChE having interacted residues depiction and Donepezil is highlighted in blue color.

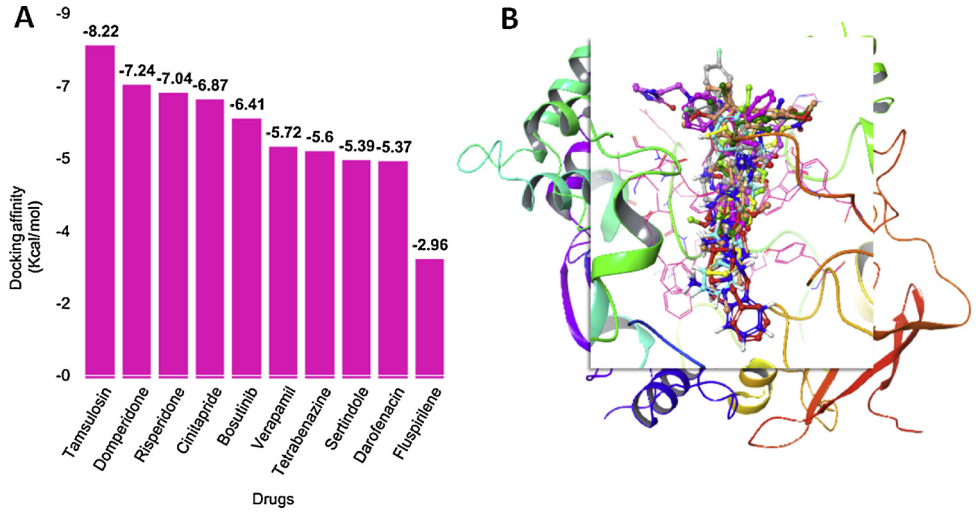

Fig. 4. A) Superimposition of all screened drugs and **B**) Glide score of all screened drugs against AChE.

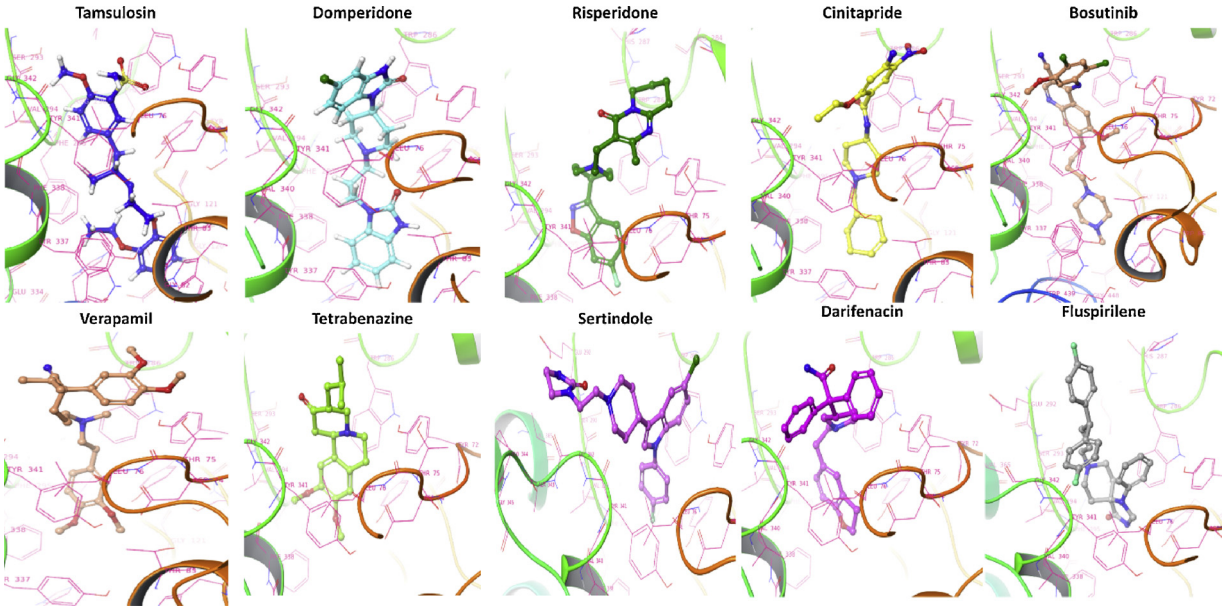

Fig. 5. Docking complexes of all screened drugs.

around the risperidone are Asp74, Leu76, Tyr124, Phe338, Phe297, Val294, Ser293, His287, Trp286 and Asn283. The Cinitapride docking complex single interaction was observed against Trp286. The attachment of bulky group (nitro, amino and ethoxy) on benzene ring causes hindrance in its penetration towards binding pocket and present at the opening position of cavity. Whereas, the other simple benzene of Cinitapride showed its penetration inside the binding cavity due to absence of such bulky groups. The aromatic ring of substituted of benzamide interact with Trp286 by π-π stacking interaction. Existing data also ensure the significance of Trp286 in different inhibitors binding which is good correlation of our docking results [53]. The graphical depiction of both docking complexes are mentioned in Fig. 5 and their 2D depiction in supplementary data Figure S4.

3.9. Bosutinib and verapamil binding analysis

Bosutinib and verapamil docked complexes were evaluated to check their binding conformations and interaction pattern within the active binding site of AChE. Bosutinib binds inside active binding pocket of target protein. In Bosutinib docking, no interaction was observed however, the surrounded residues were similar to binding pocket of donepezil-AChE complex. However, in verapamil docking single interaction was observed between di-methoxy phenyl ring and aromatic residue Tyr341. In Verapamil, two methoxy phenyl rings are attached at terminal positions of the molecule. One terminal part of verapamil contain di-methoxy phenyl ring showed their entrance within the active region of target protein. Whereas, other di-methoxy phenyl ring having couple of bulky group such as iso-propyl and cyano resist to gain penetration inside the active region of target protein. In both docking complexes most of residues were common around the drugs. Prior docking and in vitro results also show good correlation with our docking results [54,55]. The graphical depiction of both docking complexes are mentioned in Fig. 5 and their 2D depiction in supplementary data Figure. S5.

3.10. Tetrabenazine and Sertindole binding analysis

Tetrabenazine and Sertindole docked complexes were examined to interpret the binding conformations pattern within the active region of AChE. In Tetrabenazine docking single interaction was observed

between di-methoxy phenyl ring of Tetrabenazine and Trp286. In Sertindole docking couple of interactions were observed between Sertindole and amino acids. The nitrogen of five membered ring structure showed interaction against Glu292 and fused benzene ring forms π-π stacking interaction with Trp286. In both docking results Trp286 was common in interaction pattern. Prior research also ensured the importance of these residues in bonding with other AChE inhibitors which strengthen our docking results [53]. The graphical depiction of both docking complexes are depicted in Fig. 5 and their 2D depiction in supplementary data Figure S6.

3.11. Darifenacin and fluspirilene binding analysis

Darifenacin and Fluspirilene docked complexes were examined to understand the conformations pattern of both drugs within the active region of target protein. In Darifenacin docking not exact interaction was observed however, the surrounded residues were similar to binding pocket of donepezil-AChE complex. In Fluspirilene docking, two interactions were observed between drug and corresponding residues. The 4-imidazolidinone ring structure is attached with two functional moieties carbonyl and phenyl ring which are involved in Phe295 and Trp286 respectively. Existing data also ensured the importance of these residues in bonding with other AChE inhibitors which strengthen our docking results [56]. The graphical depiction of both docking complexes are depicted in Fig. 5 and their 2D depiction in supplementary data Figure S7.

3.12. Screened drugs and their possible involvement in different diseases

On the basis of similarity scores, VINA and Glide docking energy results, ten drugs Bosutinib, Cinitapride, Darifenacin, Domperidone, Fluspirilene, Risperidone, Sertindole, Tamsulosin, Tetrabenazine and Verapamil were selected and evaluated for binding pattern analysis against AChE. It was observed that all drugs showed good interactive behaviour within active region of target protein. Before going to further analysis, we discuss prior studies to check the functional features and their involvement in different diseases. SKI-606 (Bosutinib), synthetic quinolone derivative and selectively Src family kinase inhibitor, on human cancer cells derived from breast cancer patients to assess its potential for breast cancer treatment [57]. Cinitapride is a gastroprokinetic agent and antiulcer agent of the benzamide class and acts as an agonist of the 5-HT1 and 5-HT4 receptors and as an antagonist of the 5-HT2 receptors [58,59]. Darifenacin is an anticholinergic and antispasmotic agent used to treat urinary incontinence and overactive bladder syndrome [60]. Domperidone is a specific blocker of dopamine receptors [61,62]. Fluspirilene is a long-acting injectable antipsychotic agent used for chronic schizophrenia [63]. Risperdone and sertindole are also involved in the treatment of schizophrenia [64,65]. Tamsulosin is an alpha-adrenergic blocker used in symptomatic benign prostatic hyperplasia and urinary retention [66]. Tetrabenazine is a drug formerly used as an antipsychotic and treatment of various movement disorders [67]. Verapamil is mostly helpful in migraines and cluster headaches [68,69]. The overview description of all drugs is mentioned in Table 3.

3.13. Pharmacogenomics analysis of screened drugs

The screened drugs having good docking results were further analysed for pharmacogenomics analysis. Pharmacogenomics aims to develop rational means to optimize drug therapy, with respect to the patients' genotype, to ensure maximum efficacy with minimal adverse effects [70]. In our computational analysis couple of databases were used to predict the possible links of screened drugs with their respective genes. In Bosutinib-genes network, 85 genes were observed and 35 genes were associated with AD, which was confirmed from literature data. Similarly, in Fluspirilene-genes network total 84 genes were found and 35 were involved in different AD. The drug-genes network depiction is mentioned in Supplementary data Figure 8.

Table 3
Selected drugs and their involvement in diseases.

No	Drugs	Functions	Diseases
1	Bosutinib	Tyrosine kinase inhibitor	Cancer
2	Cinitapride	Antiulcer agent	Ulcer
3	Darifenacin	M3 muscarinic ACh receptor	Urinary incontinence
4	Domperidone	Dopamine D2 receptor antagonist	Gastroesophageal reflux
5	Fluspirilene	Antipsychotic drug	Schizophrenia
6	Risperidone	Antipsychotic medication	Schizophrenia, bipolar disorder,
7	Sertindole	Antipsychotic medication	Schizophrenia
8	Tamsulosin	Benign prostatic hyperplasia	Urinary retention
9	Tetrabenazine	Anti-chorea agent	Movement disorders
10	Verapamil	Treatment of high blood pressure	Migraines

In Domperidone gene network complex 79 genes were observed involved in different diseases. Among 79, 28 genes were involved in AD pathogenesis by some means. For risperidone, 62 genes showed their association, however, 36 genes were associated with AD by one or other means. The network depiction of both drugs is mentioned in Supplementary Figure 9. The Verapamil and Sertindole also showed their association with different genes listed in Supplementary Fig. 10. From both drug-genes networks 11 genes were associated with AD.

Tetrabenazine, Darifenacin, Cinitinib and Tamsulosin drugs showed associations with fewer genes compared to others. Tetrabenazine form interaction with three, Darifenacin with six, while Cinitapride and Tamsulosin form association with 3 genes each (Supplementary Figure 11). Amongst all, DRD2, SLC18A2, CHRM2, CYP3A4, ADRA1A/B, and ADRA1D genes were associated with AD.

To verify our predicted pharmacogenomics networks, a detail data mining analysis was performed on each gene to check their association with AD (Table 4). Among all drug-genes networks few common AD associated genes were observed which strengthen our proposed drug-repositioning hypothesis. Moreover, Cinitapride, Risperidone, Domperidone, Tamsulosin and Verapamil associated genes showed good connection with AD compared to other drug-genes networks. Therefore, these drugs were further employed MD simulation and *in vitro* experiments.

3.14. Molecular dynamic simulation

Based on docking and pharmacogenomics results, Cinitapride, Risperidone, Domperidone, Tamsulosin and Verapamil docked complexes were selected to evaluate the residual flexibility in the target protein. The MD simulation study was employed at 30 ns by using Gromacs 4.5.4 tool to generate root mean square deviations (RMSD), root mean square fluctuations (RMSF), solvent accessible surface area (SASA) and radius of gyration (Rg) graphs.

3.15. Root mean square deviation and fluctuations

The RMSD and RMSF graphs were generated to understand the protein backbone behavior in the simulation running time period. The RMSD results showed that in all five docked complexes, protein backbone deviation remained steady stable with the passage of simulation time frame 0–30 ns. All the graph lines displayed an increasing trend with RMSD values ranging from 0.1 to 0.3 nm from 0 to 30,000 ps.

Initially, all the graph lines (green, violet, cyan, pink and red) of all docked complexes showed a little increasing trend with RMSD value 0.1-0.2 nm. from 0 to 5,000 ps all the complexes were stable having

Table 4
Screened drugs in association with AD genes.

Drugs	AD gene with references
Bosutinib	DDR1/2 [71], SRC [72], AAK1 [73], CDH1 [74–76], BTK [77], CAMK1D [78], CAMKK2 [79,80], CLK1/3 [81], ERBB2-4 [82], EPHA4-6 [83], MAPK4/6 [84,85], MAST1 [86], NTRK1/2 [87], NUAK2 [88,89], PAK1/3 [90], PLK2 [91], PRKCD [92], PTK2 [93], PTK2B [94,95], ROCK1/2 [96], SIK1 [97], FYN [98], GRK4 [99], HCK [100], HIPK1/4 [101], IRAK1/4 [102], JAK2 [103], LCK [104], LRRK2 [105], LYN [106], MAP2K1/2/5 [107], SYK [108], TYRO3 [109], ULK2/3 [110], WEE1/2 [111]
Domperidone	ACTB [112,113], ANAPC5 [114], ANP32 A [115], ENO1 [116], GDI2 [117], GNB5 [118], PICALM [119,1], POLR2E [120], RAB5/A [121], SPTLC1 [122,123], SRSF1 [124,125], STIP1 [126], TMEM230 [127,128], CTGF [129], CXCL1 [130], CXCL8 [131–133], HMOX1 [134], ICAM1 [135,136], NAV3 [137], PTGS2 [138,139], TGFB2 [140], THBS1 [141], ABCB1 [142] CYP2D6 [143], CYP3A4 [144], IL6 [145], TGFB1 [146], DRD2/3 [147]
Verapamil	ABCB1 [148], ADRA2A [149,150], DRD3 [151], HTR2A [152], ATM [153], AP3K7 [154], NDFIP1 [155], NRIP1 [156], RAN [157], STAT1 [158], EID1 [159]
Tetrabenazine	DRD2 [147], SLC18A2 [160]
Tamsulosin	ADRA1A [149,150], ADRA1B [161], ADRA1D [162]
Sertindole	AR [163], ESR1 [164], HTR1E [165,166], HTR2A [152], HTR2C [167], DRD2 [147]
Risperidone	ADRA1A/D [149,150], ADRA2A/B/C [161,162], CHRM1/2 [143,168], CYP2D6 [169,143], DRD1/2/3/4 [147,151], HRH1/2 [170], HTR6 [171], HTR7 [172], CYP2D6 [169,143], DRD2 [148] AATF [173], ATP8A2 [174], BDNF-AS [175], CNR1 [176], CYGB [177], DDR2 [71,178], DRD3 [151], FGA [179], HTR2A [152], HTR2C [167], IL6 [180,145], LEP [181,182], TNF [183], CYP2D6 [169,143], DRD1/2/3 [147,151], ABCB1 [142,148], ABCG2 [184], BDNF [185], CASP3 [186], CASP7 [187], CRH [188], CYP3A4/5 [189], HMGCR [190], MAOA [191], SNAP25 [192]
Fluspiriline	DRD2/3 [147], ADRB2 [193], AR [163], CYP2D6 [143], HCRTR1 [194], HTR1E [165,166], HTR2A [152], HTT [195], MDM4 [196], OPRD1 [197], PPARD [198], PPARG [199], PPP1CA [200], SMAD3 [146], STK33 [201], THPO [202], XBP1 [203], KDM4 A [204], ATF3 [205], CASP2 [206], EGR1 [207], FOS [208], GADD45 A [209], HERPUD1 [210], HMGCR [211], HMGCS1 [212], HMOX1 [134], IRF1 [213], JUN [214], KLF2 [215], LDLR [216], MT1G [217,218], RCAN1 [219], TRIB1/3 [220], VEGFA [221]
Cinitapride	CYP3A4 [144]
Darifenacin	CHRM2 [222]

RMSD value 0.25 nm. However, in risperidone and Domperidone complexes, the graph lines (green and violet) showed little fluctuations respectively, while all others (Verapamil, Tamsulosin and Cinitapride) remain stable. In this time period the RMSD graphs lines showed static behavior in protein backbone and no high fluctuations were observe at 5000 nm. From 5,000–10,000 ps, Domperidone showed little upward fluctuations and showed 0.3 nm RMSD value. However, at same time risperidone showed downward fluctuations. While rest of all three graph lines (cyan, pink and red) remain static behavior having RMSD value 0.25 nm.

From 10,000–20,000 ps simulation time, a static and non-fluctuated trend was observed in all docked complexes. Both risperidone and Domperidone attained static behavior at 0.25 nm as like other three Verapamil, Tamsulosin and Cinitapride complexes. The overall RMSD graphs lines showed that all complexes were remains stable and less fluctuated upto 20,000 ps. After that from 20,000 to 30,000 ps simulation time frame same trend was seen in all five docked complexes and no fluctuations were observed. The generated graphs results showed the stable behavior in the backbone of all protein complexes. Results showed that the binding of all these drugs did not affect the structural configurations of target protein and backbone of AChE remains stable in the simulation time (Fig. 6A).

The RMSF results of all five docked structures (green, violet, cyan, pink and red) dynamically fluctuated from residues N to C terminals. Three higher fluctuation peaks were observed with RMSF value range from 0.6-0.7 nm at C-terminal region. These fluctuated peaks represents loop regions in protein structures. Risperidone, Cinitapride and Verapamil loops structure showed 0.6, 0.6 and 0.7 nm values. However, risperidone complex attained RMSF value 0.5 (Fig. 6B).

3.16. Solvent accessible surface area and radius of gyration

The structural compactness of protein was calculated by radius of gyration (Rg). The generated results depicted that Rg values of all the docked structures showed little variations from 2.22 to 2.26 nm. Initially, the graph lines were not much stable and showed little fluctuations from 0 to 5,000 ps while after that stable behaviour with little fluctuations was observed from 5,000–10,000 ps time scale. After that, no bigger fluctuations were observed in graphs lines and Rg value also remained stable at 2.24 nm except Risperidone complexes. The risperidone complex showed more fluctuations from 20000 to 30000 ps and value stable at 2.20 nm. The comparative results showed that all docked complexes were stable except the Risperidone which showed little variations (Fig. 6C). The solvent-accessible surface areas (SASA) were also observed and shown in (Fig. 6D). Results showed that the values of SASA of all five docked complexes were centered on 165 nm^2 in the simulation time 0–30000 ps.

3.17. AChE inhibition evaluations

The best five (Risperidone, Domperidone, Verapamil, Tamsulosin and Cinitapride) screened drugs were selected to check the inhibitory potential AChE. The enzyme inhibitory results showed that all selected drug inhibition potential against AChE with IC_{50} values, which validate our computational hypothesis. The comparative analysis showed that among all five drugs Cinitapride exhibited better therapeutic potential having (IC_{50} = 0.11 ± 0.01) compared to standard Neostigmine methylsulfate with (IC_{50} = 2.03 ± 0.05) whereas, less active compare to donepezil (IC_{50} = 0.006 ± 0.003). The Risperidone also possessed good comparable inhibitory potential having IC_{50} = 7.28 ± 0.37 compared to standard compound. The predicted results justified that Cinitapride possessed good inhibitory potential against AChE as compared to all other drugs and can be used as new therapeutic agent in the treatment of AD (Table 5).

In our computational approach, five drugs were proposed which seem to be active against AChE. The screened drugs were tested against AChE and showed good inhibitory activity as mentioned in Table 5. However, the best drug (Cinitapride) which showed better inhibition compared to standard (Neostigmine methylsulfate) and displayed non-competitive behaviour. In docking approach we restricted our ligands into specific grid site therefore, all ligands were binds in this selected position. There are multiple examples are available in which inhibitors computationally binds within active region of target protein whereas, their behaviour in kinetic mechanism is non-competitive inhibition [55,223].

3.18. Kinetic mechanism

To better understand the mechanistic insight of Cinitapride against AChE, a detail kinetic mechanism inhibition study was performed and evaluates its binding pattern. Based on our IC_{50} results, we selected the most potent Cinitapride to determine their inhibition type and inhibition constant on AChE enzyme. The inhibitory potential of Cinitapride against free enzyme (AChE) and enzyme substrate complex was

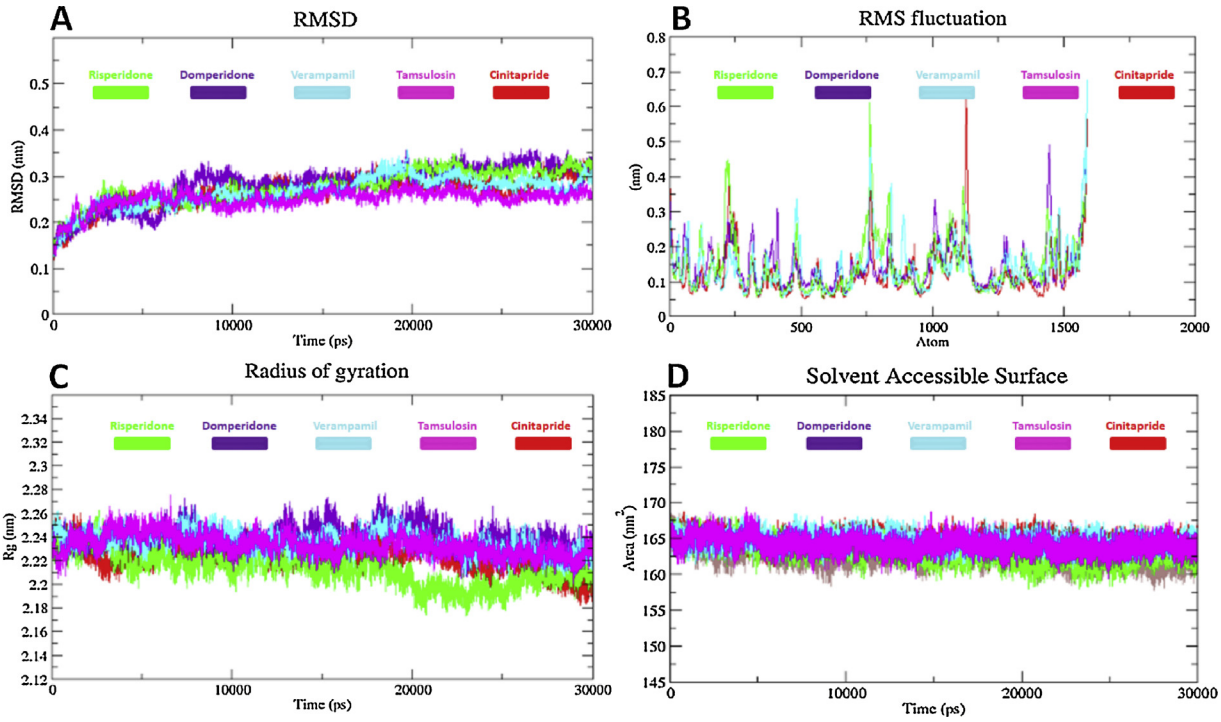

Fig. 6. A, B, C, D) RMSD/F, Rg and SASA graphs of all the docking structures from 0 to 30000 ps simulation time frame.

Table 5
IC_{50} values of selective drugs against AChE.

Selective Drugs	AChE (IC_{50} ± SEM (μM)
Risperidone	7.28 ± 0.37
Domperidone	58.23 ± 3.50
Verapamil	60.04 ± 1.25
Tamsulosin	81.84 ± 6.43
Cinitapride	0.11 ± 0.01
Neostigmine methylsulfate	2.03 ± 0.05
Donepezil	0.006 ± 0.003

Values are expressed as mean ± SEM; SEM = Standard Error of Mean.

Table 6
Kinetic parameters of Cinitapride on AChE.

Concentration (μM)	V_{max} (ΔA /Sec)	Km (mM)	Inhibition Type	*Ki* (μM)
0.00	0.001868	1.43	Non-Competitive	0.045
0.0586	0.000268303	1.43		
0.1172	0.000193636	1.43		
0.2344	0.000149788	1.43		

V_{max} is the reaction velocity, Km is the Michaelis-Menten constant, *Ki* is the EI dissociation constant.

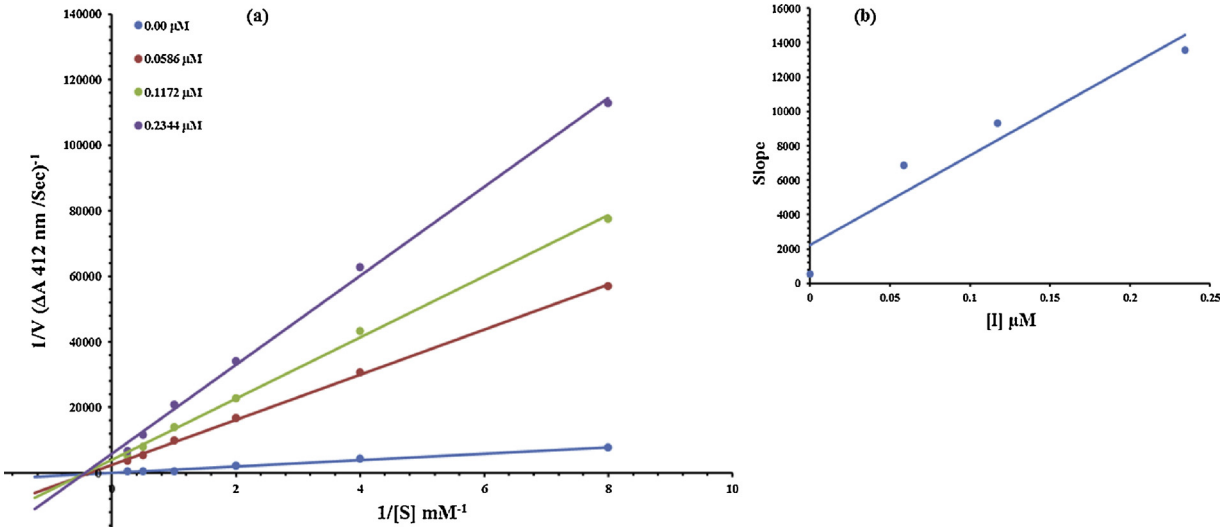

Fig. 7. Lineweaver-Burk plots for inhibition of acetylcholine esterase from human erythrocytes in the presence of inhibitor Cinitapride (**a**) Concentrations of Cinitapride were 0.00, 0.0586, 0.1172 and 0.2344 μM, Substrate acetylthiocholine iodide concentrations were 4, 2, 1, 0.5, 0.25, and 0.125 mM. (**b**) The insets represent the plot of the slope.

determined in terms of EI and ESI constants, respectively. The kinetic studies of the enzyme by the Lineweaver-Burk plot of 1/V versus 1/[S] in the presence of different Cinitapride concentrations gave a series of straight lines (Fig. 7a). The generated results showed that Cinitapride intersected within the second quadrant in Lineweaver-Burk plot. The analysis showed that V_{max} decreased to new increasing doses of Cinitapride on the other hand K_m remains same with constant value 1.43 mM. This behaviour indicates that drug Cinitapride inhibit the AChE non-competitively to form enzyme inhibitor complex. Secondary plot of slope against the concentrations of inhibitor showed enzyme inhibitor dissociation constant (K*i*) (Fig. 7b). The kinetic results are presented in the Table 6.

4. Conclusion

Molecular docking has been widely used for drug discovery [224–228]. Current study evaluates the repositioning of known drugs for AD using both computational and enzyme inhibitory kinetic approaches. The computational shaped-based screening results showed that from 1516 FDA approved drugs, 36 were displayed good structural similarity with standard template donepezil. Moreover, docking profile and pharmacogenomics evaluations depicted that from the bunch of 36 only five drugs were most active and showed good results compared to other drugs. The MD simulation results exposed that these five drugs (Risperidone, Domperidone, Verapamil, Tamsulosin and Cinitapride) showed better profiles with respect to their RMSD, RMSF, SASA and Rg evaluations graphs and steadily stable behaviour was observed in all docking complexes. The enzyme inhibition and kinetic mechanism of these drugs showed that Cinitapride has good therapeutic potential with respect to standard and other drugs. Based on aforementioned results, it is concluded that Cinitapride has better repositioning profile which may be used in the treatment of AD after clinical assessment.

Acknowledgements

The present study was supported by Basic Science Research Program through the National Research Foundation of Korea (NRF) funded by the Ministry of Education, Republic of Korea (2017R1D1A1B03034948).

Appendix A. Supplementary data

Supplementary material related to this article can be found, in the online version, at doi:https://doi.org/10.1016/j.biopha.2018.11.115.

References

[1] A.A. Moustafa, et al., Genetic underpinnings in Alzheimer's disease - a review, Rev. Neurosci. 29 (2018) 21–38.
[2] A. Zabłocka, Alzheimer's disease as neurodegenerative disorder, Postepy. Hig. Med. Dosw. 60 (2006) 209–216.
[3] C. Qiu, et al., Epidemiology of Alzheimer's disease: occurrence, determinants, and strategies toward intervention, Dialogues Clin. Neurosci. 11 (2009) 111–128.
[4] K.H. Ashe, K.R. Zahs, Probing the biology of Alzheimer's disease in mice, Neuron 66 (2010) 631–645.
[5] Y. Huang, L. Mucke, Alzheimer mechanisms and therapeutic strategies, Cell 148 (2012) 1204–1222.
[6] H.W. Querfurth, F.M. LaFerla, Alzheimer's disease, New England J. Med. Surg. Collat. Branches Sci. 362 (2010) 329–344.
[7] J.K. Yella, et al., Changing trends in computational drug repositioning, Pharmaceuticals 11 (2018) E57.
[8] A.B. Nagaraj, et al., Using a novel computational drug-repositioning approach (DrugPredict) to rapidly identify potent drug candidates for cancer treatment, Oncogene 37 (2018) 403–414.
[9] H.A. Ghofrani, et al., Sildenafil: from angina to erectile dysfunction to pulmonary hypertension and beyond, Nat. Rev. Drug Discov. 5 (2006) 689–702.
[10] S. Joglekar, M. Levin, The promise of thalidomide: evolving indications, Drugs Today 40 (2004) 197–204.
[11] F. Hefti, et al., The case for soluble Aβ oligomers as a drug target in Alzheimer's disease, Trends Pharmacol. Sci. 34 (2013) 261–266.
[12] M.S. Rafii, P.S. Aisen, Advances in Alzheimer's disease drug development, BMC Med. 13 (2015) 62.
[13] J. Nasica-Labouze, et al., Amyloid β protein and alzheimer's disease: when computer simulations complement experimental studies, Chem. Rev. 115 (2015) 3518–3563.
[14] M.A. Abbasi, et al., Synthesis, enzyme inhibitory kinetics mechanism and computational study of N-(4-methoxyphenethyl)-N-(substituted)-4-methylbenzenesulfonamides as novel therapeutic agents for Alzheimer's disease, PeerJ 6 (2018) e4962.
[15] M. Cygler, et al., Relationship between sequence conservation and three-dimensional structure in a large family of esterases, lipases and related proteins, Protein Sci. 2 (1993) 366–382.
[16] V. Tougu, Acetylcholinesterase: mechanism of catalysis and inhibition, Curr. Med. Chem. 1 (2001) 155–170.
[17] M. Mehta, et al., New acetylcholinesterase inhibitors for Alzheimer's disease, Int. J. Alzheimers Dis. 2012 (2012) 728983.
[18] J.H. Lee, et al., Donepezil across the spectrum of Alzheimer's disease: dose optimization and clinical relevance, Acta Neurol. Scand. 131 (2015) 259–267.
[19] C.H. Rojas-Fernandez, Successful use of donepezil for the treatment of dementia with Lewy bodies, Ann. Pharmacother. 35 (2001) 202–205.
[20] R. Malouf, J. Birks, Donepezil for vascular cognitive impairment, Cochrane Database Syst. Rev. 2004 (2004) CD004395.
[21] E.F. Pettersen, et al., UCSF Chimera–a visualization system for exploratory research and analysis, J. Comput. Chem. 25 (2006) 1605–1612.
[22] L. Willard, et al., VADAR: a web server for quantitative evaluation of protein structure quality, Nucleic Acids Res. 31 (2003) 3316–3319.
[23] Studio Discovery, DS Visualizer and ActiveX Control, (2008).
[24] A. Nordberg, A.L. Svensson, Cholinesterase inhibitors in the treatment of Alzheimer's disease: a comparison of tolerability and pharmacology, Drug Saf. 19 (1998) 465–480.
[25] V. Zoete, et al., SwissSimilarity: a web tool for low to ultra high throughput ligand-based virtual screening, J. Chem. Inf. Model. 56 (2016) 1399–1404.
[26] W.L. DeLano, Pymol: an open-source molecular graphics tool, CCP4 Newslett. Protein Crystallogr. 40 (2002) 82–92.
[27] S. Dallakyan, A.J. Olson, Small-molecule library screening by docking with PyRx, Methods Mol. Biol. 1263 (2015) 243–250.
[28] G.M. Sastry, et al., Protein and ligand preparation: parameters, protocols, and influence on virtual screening enrichments, J. Comput. Aid. Mol. Des 27 (2013) 221–234.
[29] J. Cheung, et al., Structures of human acetylcholinesterase in complex with pharmacologically important ligands, J. Med. Chem. 55 (2012) 10282–10286.
[30] R.A. Friesner, et al., Extra precision glide: docking and scoring incorporating a model of hydrophobic enclosure for protein-ligand complexes, J. Med. Chem. 49 (2006) 6177–6196.
[31] R. Farid, et al., New insights about HERG blockade obtained from protein modeling, potential energy mapping, and docking studies, Bioorg. Med. Chem. 14 (2006) 3160–3173.
[32] S. Pronk, et al., GROMACS 4.5: a high-throughput and highly parallel open source molecular simulation toolkit, Bioinformatics 29 (2013) 845–854.
[33] S.W. Chiu, et al., An improved united atom force field for simulation of mixed lipid bilayers, J. Phys. Chem. B 113 (2009) 2748–2763.
[34] H. Wang, et al., Optimizing working parameters of the smooth particle mesh Ewald algorithm in terms of accuracy and efficiency, J. Chem. Phys. 133 (2010) 034117.
[35] S. Amiri, M.S. Sansom, P.C. Biggin, Molecular dynamics studies of AChBP with nicotine and carbamylcholine: the role of water in the binding pocket, Protein Eng. Des. Sel. 20 (7) (2007) 353–359.
[36] K.C. Cotto, et al., DGIdb 3.0: a redesign and expansion of the drug-gene interaction database, Nucleic Acids Res. 46 (January (D1)) (2018) D1068–D1073.
[37] M. Yoo, et al., DSigDB: drug signatures database for gene set analysis, Bioinformatics 31 (2015) 3069–3071.
[38] P. Shannon, et al., Cytoscape: a software environment for integrated models of biomolecular interaction networks, Genome Res. 13 (2003) 2498–2504.
[39] G.L. Ellman, et al., A new and rapid colorimetric determination of acetylcholinesterase activity, Biochem. Pharmacol. 7 (1961) 88IN191-9095.
[40] M. Saleem, et al., Facile synthesis, crystal structure, DFT calculation and biological activities of 4-(2-fluorophenyl)-3-(3-methoxybenzyl)-1H-1, 2, 4-triazol-5 (4H)-one (5), Med. Chem. (Los Angeles) 14 (2018) 451–459.
[41] M. Saleem, et al., Synthesis, urease and acetylcholine esterase inhibition activities of some 1, 4-disubstituted thiosemicarbazides and their 2, 5-disubstituted thiadiazoles, Bull. Korean Chem. Soc. 33 (2012) 2741–2747.
[42] D.L. Ma, et al., Drug repositioning by structure-based virtual screening, Chem. Soc. Rev. 42 (2013) 2130–2141.
[43] E. March-Vila, et al., On the integration of in silico drug design methods for drug repurposing, Front. Pharmacol. 8 (2017) 298.
[44] M. Hassan, et al., Molecular docking and dynamic simulation of AZD3293 and solanezumab effects against BACE1 to treat alzheimer's disease, Front. Comput. Neurosci. 12 (2018) 34.
[45] M. Hassan, et al., Exploration of novel human tyrosinase inhibitors by molecular modeling, docking and simulation studies, Interdiscip. Sci. 10 (2018) 68–80.
[46] M. Hassan, et al., Exploring the mechanistic insights of Cas scaffolding protein family member 4 with protein tyrosine kinase 2 in Alzheimer's disease by evaluating protein interactions through molecular docking and dynamic simulations, Neurol. Sci. 39 (2018) 1361–1374.
[47] M. Hassan, et al., Investigation of Klotho-FGF21 complex as a target of metabolic disorder through molecular docking and simulation studies, JSM Biochem. Mol. Biol. 4 (2017) 1024.

[48] I. Silman, J.L. Sussman, Acetylcholinesterase: how is structure related to function? Chem. Biol. Interact. 175 (2008) 3–10.
[49] Y. Zhou, et al., Catalytic reaction mechanism of acetylcholinesterase determined by Born-Oppenheimer ab initio QM/MM molecular dynamics simulations, J. Phys. Chem. B 114 (2010) 8817–8825.
[50] R.A. Friesner, et al., Glide: a new approach for rapid, accurate docking and scoring. 1. Method and assessment of docking accuracy, J. Med. Chem. 47 (2004) 1739–1749.
[51] T.A. Halgren, et al., Glide: a new approach for rapid, accurate docking and scoring. 2. Enrichment factors in database screening, J. Med. Chem. 47 (2004) 1750–1759.
[52] M. Pohanka, P. Dobes, Caffeine inhibits acetylcholinesterase, but not butyrylcholinesterase, Int. J. Mol. Sci. 14 (2013) 9873–9882.
[53] S. Simeon, et al., Probing the origins of human acetylcholinesterase inhibition via QSAR modeling and molecular docking, PeerJ 4 (2016) e2322.
[54] S.H. Lu, et al., The discovery of potential acetylcholinesterase inhibitors: a combination of pharmacophore modeling, virtual screening, and molecular docking studies, J. Biomed. Sci. 18 (2011) 8.
[55] J. Fang, et al., Inhibition of acetylcholinesterase by two genistein derivatives: kinetic analysis, molecular docking and molecular dynamics simulation, Acta Pharm. Sin. B 4 (2014) 430–437.
[56] L. Zhang, et al., Identification of human acetylcholinesterase inhibitors from the constituents of EGb761 by modeling docking and molecular dynamics simulations, Comb. Chem. High Throughput Screen. 21 (2018) 41–49.
[57] A. Vultur, et al., SKI-606 (bosutinib), a novel Src kinase inhibitor, suppresses migration and invasion of human breast cancer cells, Mol. Cancer Ther. 7 (2008) 1185–1194.
[58] Romero C. Alarcón-de-la-Lastra, et al., Cinitapride protects against ethanol-induced gastric mucosal injury in rats: role of 5-hydroxytryptamine, prostaglandins and sulfhydryl compounds, Pharmacol 54 (1997) 193–202.
[59] C. Alarcón de la Lastra, et al., Effects of cinitapride on gastric ulceration and secretion in rats, Inflamm. Res. 47 (1998) 131–136.
[60] K. Hesch, Agents for treatment of overactive bladder: a therapeutic class review, Proc 20 (2007) 307–314.
[61] J.A. Barone, Domperidone: a peripherally acting dopamine2-receptor antagonist, Ann. Pharmacother. 33 (1999) 429–440.
[62] S.C. Reddymasu, et al., Domperidone: review of pharmacology and clinical applications in gastroenterology, Am. J. Gastroenterol. 102 (2007) 2036–2045.
[63] J.H. van Epen, Experience with fluspirilene (R 6218), a long-acting neuroleptic, Psychiatr. Neurol. Neurochir. 73 (1970) 277–284.
[64] Janssen Pharmaceuticals, Inc, Risperdal (Risperidone) Tablets and Oral Solution and Risperdal M-Tab (Risperidone) Orally Disintegrating Tablets Prescribing Information, Titusville, NJ (2014).
[65] R. Lewis, et al., Sertindole for schizophrenia, Cochrane Database Syst. Rev. 20 (2005) CD001715.
[66] R.C. Wang, et al., Effect of Tamsulosin on stone passage for ureteral stones: a systematic review and meta-analysis, Ann. Emerg. Med. 69 (2005) 353–361.
[67] C. Kenney, et al., Long-term tolerability of tetrabenazine in the treatment of hyperkinetic movement disorders, Mov. Disord. 22 (2007) 193–197.
[68] P.C. Tfelt-Hansen, R.H. Jensen, Management of cluster headache, CNS Drugs 26 (2012) 571–580.
[69] K. Merison, H. Jacobs, Diagnosis and treatment of childhood migraine, Curr. Treat. Options Neurol. 18 (2016) 48.
[70] L. Becquemont, Pharmacogenomics of adverse drug reactions: practical applications and perspectives, Pharmacogenomics. 10 (2009) 961–969.
[71] M. Hebron, et al., Discoidin domain receptor inhibition reduces neuropathology and attenuates inflammation in neurodegeneration models, J. Neuroimmunol. 311 (2017) 1–9.
[72] G. Dhawan, C.K. Combs, Inhibition of Src kinase activity attenuates amyloid associated microgliosis in a murine model of Alzheimer's disease, J. Neuroinflammation 9 (2012) 117.
[73] A.F. Abdel-Magid, Inhibitors of adaptor-associated kinase 1 (AAK1) may treat neuropathic pain, schizophrenia, parkinson's disease, and other disorders, ACS Med. Chem. Lett. 8 (2017) 595–597.
[74] A. El-Amraoui, C. Petit, Cadherins as targets for genetic diseases, Cold Spring Harb. Perspect. Biol. 2 (2010) a003095.
[75] P. Polakis, Wnt signaling and cancer, Genes Dev. 14 (2000) 1837–1851.
[76] W.J. Nelson, R. Nusse, Convergence of wnt, ß-Catenin, and cadherin pathways, Science 303 (2004) 1483–1487.
[77] G. Singhal, et al., Inflammasomes in neuroinflammation and changes in brain function: a focused review, Front. Neurosci. 8 (2014) 315.
[78] C.S. Floudas, et al., Identifying genetic interactions associated with late-onset Alzheimer's disease, BioData Min. 7 (2014) 35.
[79] G. Mairet-Coello, et al., The CAMKK2-AMPK kinase pathway mediates the synaptotoxic effects of Aβ oligomers through Tau phosphorylation, Neuron 78 (2013) 94–108.
[80] R. Nancy, Gough Pathway of Neurotoxicity, Sci. Signal. 6 (April (271)) (2013) ec85.
[81] P. Jain, et al., Human CDC2-like kinase 1 (CLK1): a novel target for Alzheimer's disease, Curr. Drug Targets 15 (2014) 539–550.
[82] B.J. Wang, et al., ErbB2 regulates autophagic flux to modulate the proteostasis of APP-CTFs in Alzheimer's disease, Proc. Natl. Acad. Sci. U. S. A. 114 (2017) 3129–3138.
[83] A.F. Rosenberger, et al., Altered distribution of the EphA4 kinase in hippocampal brain tissue of patients with Alzheimer's disease correlates with pathology, Acta Neuropathol. Commun. 2 (2017) 79.
[84] M. Li, et al., Evolutionary history of the vertebrate mitogen activated protein kinases family, PLoS One 6 (2011) e26999.
[85] L. Munoz, A.J. Ammit, Targeting p38 MAPK pathway for the treatment of Alzheimer's disease, Neuropharmacology 58 (2010) 561–568.
[86] M. Ray, W. Zhang, Analysis of Alzheimer's disease severity across brain regions by topological analysis of gene co-expression networks, BMC Syst. Biol. 4 (2010) 136.
[87] Z. Chen, et al., Genetic association of neurotrophic tyrosine kinase receptor type 2 (NTRK2) with Alzheimer's disease, Am. J. Med. Genet. B Neuropsychiatr. Genet. 147 (2011) 363–369.
[88] H. Yoshida, M. Goedert, Phosphorylation of microtubule-associated protein tau by AMPK-related kinases, J. Neurochem. 120 (2012) 165–176.
[89] X. Sun, et al., The regulation and function of the NUAK family, J. Mol. Endocrinol. 51 (2013) 15–22.
[90] Q.L. Ma, et al., PAK in Alzheimer disease, Huntington disease and X-linked mental retardation, Cell. Logist. 2 (2012) 117–125.
[91] M.K. Mbefo, et al., Phosphorylation of synucleins by members of the Polo-like kinase family, J. Biol. Chem. 285 (2010) 2807–2822.
[92] Y.H. Hsiao, et al., The involvement of Cdk5 Activator p35 in social isolation-triggered onset of early Alzheimer's disease-related cognitive deficit in the transgenic mice, Neuropsychopharmacology 36 (2011) 1848–1858.
[93] N. Tim, et al., Adaptors for disorders of the brain? The cancer signaling proteins NEDD9, CASS4, and PTK2B in Alzheimer's disease, Oncoscience 1 (2014) 486–503.
[94] B. Padhy, et al., Pseudoexfoliation and Alzheimer's associated CLU risk variant, rs2279590, lies within an enhancer element and regulates CLU, EPHX2 and PTK2B gene expression, Hum. Mol. Genet. 26 (2017) 4519–4529.
[95] P. Dourlen, et al., Functional screening of Alzheimer risk loci identifies PTK2B as an in vivo modulator and early marker of Tau pathology, Mol. Psychiatry 22 (2017) 874–883.
[96] W. Benjamin, et al., Rho-associated protein kinase 1 (ROCK1) is increased in Alzheimer's disease and ROCK1 depletion reduces amyloid-β levels in brain, J. Neurochem. 138 (2016) 525–531.
[97] Y. Dong, et al., Neutrophil hyperactivation correlates with Alzheimer's disease progression, Ann. Neurol. 83 (2018) 387–405.
[98] H.B. Nygaard, et al., Fyn kinase inhibition as a novel therapy for Alzheimer's disease, Alzheimers Res. Ther. 6 (2014) 8.
[99] W.Z. Suo, L. Li, Dysfunction of g protein-coupled receptor kinases in alzheimer's disease, Sci. World J. 10 (2010) 1667–1678.
[100] E. Castillo, et al., Comparative profiling of cortical gene expression in Alzheimer's disease patients and mouse models demonstrates a link between amyloidosis and neuroinflammation, Sci. Rep. 7 (2017) 17762.
[101] C. Lanni, et al., Homeodomain interacting protein kinase 2: a target for Alzheimer's beta amyloid leading to misfolded p53 and inappropriate cell survival, PLoS One 5 (2010) e10171.
[102] J.J.M. Hoozemans, et al., Increased IRAK-4 kinase activity in alzheimer's disease; IRAK-1/4 inhibitor I prevents pro-inflammatory cytokine secretion but not the uptake of amyloid Beta by primary human glia, J. Clin. Cell. Immunol. 5 (2014) 243.
[103] T. Chiba, et al., Targeting the JAK2/STAT3 axis in Alzheimer's disease, Expert Opin. Ther. Targets 13 (2009) 1155–1167.
[104] E.J. Kim, et al., Alzheimer's disease risk factor lymphocyte-specific protein tyrosine kinase regulates long-term synaptic strengthening, spatial learning and memory, Cell. Mol. Life Sci. 70 (2013) 743–759.
[105] Y. Zhao, et al., LRRK2 variant associated with Alzheimer's disease, Neurobiol. Aging 32 (2011) 1990–1993.
[106] D. Liang, et al., Concerted perturbation observed in a Hub Network in alzheimer's disease, PLoS One 7 (2012) e40498.
[107] S. Jayapalan, et al., Computational identification and analysis of neurodegenerative disease associated protein kinases in hominid genomes, Genes Dis. 3 (2016) 228–237.
[108] D. Paris, et al., The spleen tyrosine kinase (Syk) regulates Alzheimer amyloid-β production and Tau hyperphosphorylation, J. Biol. Chem. 289 (2014) 33927–33944.
[109] Y. Zheng, et al., Involvement of receptor tyrosine kinase Tyro3 in amyloidogenic APP processing and β-Amyloid deposition in alzheimer's disease models, PLoS One 7 (2012) e39035.
[110] A.R.T. Silva, et al., Transcriptional alterations related to neuropathology and clinical manifestation of alzheimer's disease, PLoS One 7 (2012) e48751.
[111] A. Tomashevski, et al., Constitutive Wee1 activity in adult brain neurons with M phase-type alterations in Alzheimer neurodegeneration, J. Alzheimers Dis. 3 (2001) 195–207.
[112] P. Talwar, et al., Genomic convergence and network analysis approach to identify candidate genes in Alzheimer's disease, BMC Genomics 15 (2014) 199.
[113] M. Szymanski, et al., Alzheimer's risk variants in the clusterin gene are associated with alternative splicing, Transl. Psychiatry 1 (2011) e18.
[114] W. Kong, et al., Dynamic regulatory network reconstruction for alzheimer's disease based on matrix decomposition techniques, Comput. Math. Methods Med. 2014 (2014) 891761.
[115] G.S. Gao-Shang Chai, et al., Downregulating ANP32A rescues synapse and memory loss via chromatin remodeling in Alzheimer model, Mol. Neurodegener. 12 (2017) 34.
[116] N.R. Cutler, et al., Cerebrospinal fluid neuron-specific enolase is reduced in Alzheimer's disease, Arch. Neurol. 43 (1986) 153–154.
[117] L. Zhang, et al., Identifying Tmem59 related gene regulatory network of mouse neural stem cell from a compendium of expression profiles, BMC Syst. Biol. 5 (2011) 152.
[118] Z. Ma, et al., Orexin signaling regulates both the hippocampal clock and the

circadian oscillation of Alzheimer's disease-risk genes, Sci. Rep. 6 (2016) 36035.
[119] E.H. Kok, et al., CLU, CR1 and PICALM genes associate with Alzheimer's-related senile plaques, Alzheimers Res. Ther. 3 (12) (2011).
[120] C.M. Karch, et al., Alzheimer's disease risk polymorphisms regulate gene expression in the ZCWPW1 and the CELF1 loci, PLoS One 11 (2016) e0148717.
[121] W. Xu, et al., Dysregulation of Rab5-mediated endocytic pathways in Alzheimer's disease, Traffic 19 (2018) 253–262.
[122] H. Geekiyanage, C. Chan, MicroRNA-137/181c regulates serine palmitoyltransferase and in turn amyloid {beta}, novel targets in sporadic alzheimer's disease, J. Neurosci. 31 (2011) 14820–14830.
[123] H. Geekiyanage, et al., Inhibition of SPT reduces Aβ and tau hyperphosphorylation in a mouse model, a safe therapeutic strategy for Alzheimer's disease, Neurobiol. Aging 34 (2013) 2037–2051.
[124] W. Qian, F. Liu, Regulation of alternative splicing of tau exon 10, Neurosci. Bull. 30 (2014) 367–377.
[125] J. Jianhua Shi, et al., Cyclic AMP-dependent protein kinase regulates the alternative splicing of Tau exon 10, J. Biol. Chem. 286 (2011) 14639–14648.
[126] E. Rachel, et al., The Hsp70/Hsp90 chaperone machinery in neurodegenerative diseases, Front. Neurosci. 11 (2017) 254.
[127] S.L. Siedlak, et al., TMEM230 accumulation in granulovacuolar degeneration bodies and dystrophic neurites of alzheimer's disease, J. Alzheimers Dis. 58 (2017) 1027–1033.
[128] D. Ma, et al., Screening for TMEM230 mutations in young-onset Parkinson's disease, Neurobiol. Aging 58 (2017) e10.
[129] Z. Zhao, et al., Connective tissue growth factor (CTGF) expression in the brain is a downstream effector of insulin resistance- associated promotion of Alzheimer's disease beta-amyloid neuropathology, FASEB J. 19 (2005) 2081–2082.
[130] Y. Tamura, et al., Association study of the chemokine, CXC motif, ligand 1 (CXCL1) gene with sporadic Alzheimer's disease in a Japanese population, Neurosci. Lett. 379 (2005) 149–151.
[131] M. Fiala, et al., Amyloid-beta induces chemokine secretion and monocyte migration across a human blood-brain barrier model, Mol. Med. 4 (1998) 480–489.
[133] K. Bonotis, et al., Systemic immune aberrations in Alzheimer's disease patients, J. Neuroimmunol. 193 (2008) 183–187.
[134] H.Y. Sung, et al., Amyloid beta-mediated hypomethylation of heme oxygenase 1 correlates with cognitive impairment in alzheimer's disease, PLoS One 11 (2016) e0153156.
[135] E.M. Frohman, et al., Expression of intercellular adhesion molecule 1 (ICAM-1) in Alzheimer's disease, J. Neurol. Sci. 106 (2016) 105–111.
[136] R. Pola, et al., Intercellular adhesion molecule-1 K469E gene polymorphism and Alzheimer's disease, Neurobiol. Aging 24 (2003) 385–387.
[137] J. Satoh, MicroRNAs and their therapeutic potential for human diseases: aberrant microRNA expression in Alzheimer's disease brains, J. Pharmacol. Sci. 114 (2010) 269–275.
[138] Q. Chen, et al., Influence of four polymorphisms in ABCA1 and PTGS2 genes on risk of Alzheimer's disease: a meta-analysis, Neurol. Sci. 37 (2016) 1209–1220.
[139] M. Hassan, et al., Regulatory cascade of neuronal loss and glucose metabolism, CNS Neurol. Disord. Drug Targets 13 (2014) 1232–1245.
[140] P. Bosco, et al., Role of the Transforming-Growth-Factor-β1 gene in late-onset alzheimer's disease: implications for the treatment, Curr. Genomics 14 (2013) 147–156.
[141] S.M. Son, et al., Thrombospondin-1 prevents amyloid beta-mediated synaptic pathology in Alzheimer's disease, Neurobiol. Aging 36 (2015) 3214–3227.
[142] R. Kohen, et al., ABCB1 genotype and CSF β-Amyloid in alzheimer disease, J. Geriatr. Psychiatry Neurol. 24 (2011) 63–66.
[143] M. Gołab-Janowska, et al., CYP2D6 gene polymorphism as a probable risk factor for Alzheimer's disease and Parkinson's disease with dementia, Neurol. Neurochir. Pol. 41 (2007) 113–121.
[144] R. Cacabelos, et al., Gene interactions in the pharmacogenomics of alzheimer's disease, Int. J. Mol. Genet. Gene. Ther. 1 (1) (2015), https://doi.org/10.16966/2471-4968.102.
[145] L. Ramos Dos Santos, et al., Association study of the BIN1 and IL-6 genes on Alzheimer's disease, Neurosci. Lett. 614 (2016) 65–69.
[146] R. von Bernhardi, et al., Role of TGFβ signaling in the pathogenesis of Alzheimer's disease, Front. Cell. Neurosci. 9 (2015) 426.
[147] G.W. Small, et al., D2 dopamine receptor A1 allele in Alzheimer disease and aging, Arch. Neurol. 54 (1997) 281–285.
[148] X. Zhong, et al., Association between ABCB1 polymorphisms and haplotypes and Alzheimer's disease: a meta-analysis, Sci. Rep. 2016 (6) (2016) 32708.
[149] A.W. Butler, et al., Meta-analysis of linkage studies for Alzheimer's disease — a web resource, Neurobiol. Aging 30 (2009) 1037–1047.
[150] J.H. Lee, et al., Analyses of the national institute on aging late-onset alzheimer's disease family study: implication of additional loci, Arch. Neurol. 65 (2008) 1518–1526.
[151] D. Craig, et al., Psychotic symptoms in Alzheimer's disease are not influenced by polymorphic variation at the dopamine receptor DRD3 gene, Neurosci. Lett. 368 (2004) 33–36.
[152] J. Thome, et al., Association analysis of HTR6 and HTR2A polymorphisms in sporadic Alzheimer's disease, J. Neural Transm. Vienna (Vienna) 108 (2001) 1175–1180.
[153] X. Shen, et al., Neurons in vulnerable regions of the alzheimer's disease brain display reduced ATM signaling, eNeuro 3 (2016) 124.
[154] F. Zeidán-Chuliá, et al., Altered expression of Alzheimer's disease-related genes in the cerebellum of autistic patients: a model for disrupted brain connectome and therapy, Cell Death Dis. 5 (2016) e1250.
[155] J. Tian, et al., Lower expression of Ndfip1 is associated with alzheimer disease pathogenesis through decreasing DMT1 degradation and increasing Iron influx, Front. Aging Neurosci. 10 (2018) 165.
[156] V.A. Stepanov, et al., Replicative association analysis of genetic markers of cognitive traits with Alzheimer's disease in a Russian population, Mol. Biol. (Mosk.) 48 (2014) 952–962.
[157] D. Mastroeni, et al., Reduced RAN expression and disrupted transport between cytoplasm and nucleus; a key event in Alzheimer's disease pathophysiology, PLoS One 8 (2013) e53349.
[158] W.L. Hsu, et al., STAT1 negatively regulates spatial memory formation and mediates the memory-impairing effect of Aβ, Neuropsychopharmacology 39 (2014) 746–758.
[159] R. Liu, et al., Increased EID1 nuclear translocation impairs synaptic plasticity and memory function associated with pathogenesis of Alzheimer's disease, Neurobiol. Dis. 45 (2012) 902–912.
[160] S. Yamamoto, et al., Positive immunoreactivity for vesicular monoamine transporter 2 in Lewy bodies and Lewy neurites in substantia nigra, Neurosci. Lett. 396 (2006) 187–191.
[161] V. Giedraitis, et al., Genetic analysis of alzheimer's disease in the Uppsala longitudinal study of adult men, Dement. Geriatr. Cogn. Disord. 27 (2009) 59–68.
[162] C.J. Hong, et al., A study of alpha-adrenoceptor gene polymorphisms and Alzheimer disease, J. Neural Transm. Vienna (Vienna) 108 (2001) 445–450.
[163] R. Ferrari, et al., Androgen receptor gene and sex-specific Alzheimer's disease, Neurobiol. Aging 34 (2077) (2013) e19–20.
[164] C. Luckhaus, P.G. Sand, Estrogen Receptor 1 gene (ESR1) variants in Alzheimer's disease. Results of a meta-analysis, Aging Clin. Exp. Res. 19 (2007) 165–168.
[165] T.P. Blackburn, Serotonin (5-hydroxytryptamine; 5-HT): receptors, in: L.R. Squire (Ed.), Encyclopedia of Neuroscience, Academic Press, Oxford, UK, 2009, pp. 8770–8783.
[166] D. Hoyer, et al., Molecular, pharmacological and functional diversity of 5-HT receptors, Pharmacol. Biochem. Behav. 71 (2002) 533–554.
[167] C. Holmes, et al., 5-HT-2A and 5-HT-2C receptor polymorphisms and psychopathology in late onset Alzheimer's disease, Hum. Molec. Genet 7 (1998) 1507–1509.
[168] H.C. Liu, C.J. Hong, T.Y. Liu, C.W. Chi, S.J. Tsai, Association analysis for the muscarinic M1 receptor genetic polymorphisms and Alzheimer's disease, Dement. Geriatr. Cogn. Disord. 19 (1) (2005) 42–45 Epub 2004 Sep 21.
[169] C. Holmes, et al., Psychosis and aggression in Alzheimer's disease: the effect of dopamine receptor gene variation, J. Neurol. Neurosurg. Psychiatry 71 (2001) 777–779.
[170] F. Naddafi, A. Mirshafiey, The neglected role of histamine in Alzheimer's disease, Am. J. Alzheimers Dis. Other Demen. 28 (2013) 327–336.
[171] R. Kan, et al., Association of the HTR6 polymorphism C267T with late-onset Alzheimer's disease in Chinese, Neurosci. Lett. 372 (2004) 27–29.
[172] D. Švob Štrac, et al., The serotonergic system and cognitive function, Transl. Neurosci. 7 (2016) 35–49.
[173] Q. Guo, J. Xie, AATF inhibits aberrant production of amyloid beta peptide 1-42 by interacting directly with Par-4, J. Biol. Chem. 279 (2004) 4596–4603.
[174] S. Kim, et al., α-synuclein, Parkinson's disease, and Alzheimer's disease, Parkinsonism Relat. Disord. 10 (2004) 9–13.
[175] J. Budni, et al., The involvement of BDNF, NGF and GDNF in aging and Alzheimer's disease, Aging Dis. 6 (2015) 331–341.
[176] D. Gadzicki, et al., Frequent polymorphism in the coding exon of the human cannabinoid receptor (CNR1) gene, Mol. Cell. Probes 13 (1999) 321–323.
[177] C.A. Hundahl, et al., A gene-environment study of cytoglobin in the human and rat Hippocampus, PLoS One 8 (2013) e63288.
[178] H.Y. Sung, et al., Amyloid protein-mediated differential DNA methylation status regulates gene expression in Alzheimer's disease model cell line, Biochem. Biophys. Res. Commun. 414 (2011) 700–705.
[179] F. Song, et al., Plasma protein profiling of Mild Cognitive Impairment and Alzheimer's disease using iTRAQ quantitative proteomics, Proteome Sci. 12 (2014) 5.
[180] F. Licastro, et al., Interleukin-6 gene alleles affect the risk of Alzheimer's disease and levels of the cytokine in blood and brain, Neurobiol. Aging 24 (2003) 921–926.
[181] M.J. McGuire, M. Ishii, Leptin dysfunction and Alzheimer's disease: evidence from cellular, animal, and human studies, Cell. Mol. Neurobiol. 36 (2016) 203–217.
[182] J.M. Johnston, et al., Repositioning leptin as a therapy for Alzheimer's disease, Therapy. 8 (2011) 481–490.
[183] R.T. Perry, et al., The role of TNF and its receptors in Alzheimer's disease, Neurobiol. Aging 22 (2001) 873–883.
[184] Á. Fehér, et al., Association between the ABCG2 C421A polymorphism and Alzheimer's disease, Neurosci. Lett. 550 (2013) 51–54.
[185] L. Zhang, et al., BDNF gene polymorphisms are associated with Alzheimer's disease-related depression and antidepressant response, J. Alzheimers Dis. 26 (2011) 523–530.
[186] N. Louneva, et al., Caspase-3 is enriched in postsynaptic densities and increased in alzheimer's disease, Am. J. Pathol. 173 (2008) 1488–1495.
[187] K.L. Ayers, et al., A loss of function variant in CASP7 protects against Alzheimer's disease in homozygous APOE ε4 allele carriers, BMC Genomics 17 (2016) 445.
[188] H.U. Rehman, Role of CRH in the pathogenesis of dementia of Alzheimer's type and other dementias, Curr. Opin. Investig. Drugs 3 (2002) 1637–1642.
[189] N. Sonali, et al., Impact of CYP2D6 and CYP3A4 genetic polymorphism on combined cholinesterase inhibitors and memantine treatment in mild to moderate Alzheimer's disease, Dement. Geriatr. Cogn. Disord. 37 (2014) 58–70.
[190] V. Leduc, et al., HMGCR is a genetic modifier for risk, age of onset and MCI conversion to Alzheimer's disease in a three cohorts study, Mol. Psychiatry 20

(2015) 867–873.
[191] M. Takehashi, et al., Association of monoamine oxidase A gene polymorphism with Alzheimer's disease and Lewy body variant, Neurosci. Lett. 327 (2002) 79–82.
[192] F.R. Guerini, et al., Possible association between SNAP-25 single nucleotide polymorphisms and alterations of categorical fluency and functional MRI parameters in Alzheimer's disease, J. Alzheimers Dis. 42 (2014) 1015–1028.
[193] Y.S. Hu, et al., Analyzing the genes related to Alzheimer's disease via a network and pathway-based approach, Alzheimers Res. Ther. 9 (2017) 29.
[194] S. Gallone, et al., Is HCRTR2 a genetic risk factor for Alzheimer's disease? Dement. Geriatr. Cogn. Disord. 38 (2014) 245–253.
[195] S.K. Singhrao, et al., Huntingtin protein colocalizes with lesions of neurodegenerative diseases: an investigation in Huntington's, Alzheimer's, and Pick's diseases, Exp. Neurol. 150 (1998) 213–222.
[196] P. Katsel, et al., Cycle checkpoint abnormalities during dementia: a plausible association with the loss of protection against oxidative stress in alzheimer's disease, PLoS One 8 (2013) e68361.
[197] H. Ji, et al., Elevated OPRD1 promoter methylation in Alzheimer's disease patients, PLoS One 12 (2017) e0172335.
[198] H. Zhang, et al., Interaction between PPAR γ and SORL1 gene with late-onset alzheimer's disease in Chinese Han Population, Oncotarget 8 (2011) 48313–48320.
[199] Q. Jiang, et al., The role of peroxisome proliferator-activated receptor-gamma (PPARgamma) in Alzheimer's disease: therapeutic implications, CNS Drugs 22 (2008) 1–14.
[200] A. Miyashita, et al., Genes associated with the progression of neurofibrillary tangles in Alzheimer's disease, Transl. Psychiatry 4 (2014) e396.
[201] F. Hernandez, et al., GSK3 and tau: two convergence points in Alzheimer's disease, J. Alzheimers Dis. 33 (2013) 141–144.
[202] M. Edwards, et al., Thrombopoietin and Alzheimer's disease, Alzheimer' Dementia 9 (2013) P239.
[203] M. Cissé, et al., The transcription factor XBP1 in memory and cognition: implications in alzheimer's disease, Mol. Med. 22 (2016) 905–917.
[204] M.T. Lorbeck, et al., The histone demethylase Dmel\Kdm4A controls genes required for lifespan and male-specific sex-determination in drosophila, Gene 450 (2010) 8–17.
[205] M. Zhu, et al., Age-related brain expression and regulation of the chemokine CCL4/MIP-1β in APP/PS1 double-transgenic mice, J. Neuropathol. Exp. Neurol. 73 (2014) 362–374.
[206] P.N. Pompl, et al., Caspase gene expression in the brain as a function of the clinical progression of Alzheimer disease, Arch. Neurol. 60 (2003) 369–376.
[207] P. Renbaum, et al., Egr-1 upregulates the Alzheimer's disease presenilin-2 gene in neuronal cells, Gene 318 (2003) 113–124.
[208] L.L. Bonnycastle, et al., The c-fos gene and early-onset familial Alzheimer's disease, Neurosci. Lett. 160 (2003) 33–36.
[209] R. Torp, et al., GADD45 is induced in Alzheimer's disease, and protects against apoptosis in vitro, Neurobiol. Dis. 5 (1998) 245–252.
[210] X. Sai, et al., Endoplasmic reticulum stress-inducible protein, Herp, enhances presenilin-mediated generation of amyloid beta-protein, J. Biol. Chem. 277 (2002) 12915–12920.
[211] V. Leduc, et al., HMGCR is a genetic modifier for risk, age of onset and MCI conversion to Alzheimer's disease in a three cohorts study, Mol. Psychiatry 20 (2015) 867–873.
[212] V. Tseveleki, et al., Comparative gene expression analysis in mouse models for multiple sclerosis, Alzheimer's disease and stroke for identifying commonly regulated and disease-specific gene changes, Genomics 96 (2002) 82–91.
[213] T. Masuda, et al., Transcription factor IRF1 is responsible for IRF8-mediated IL-1β expression in reactive microglia, J. Pharmacol. Sci. 128 (2015) 216–220.
[214] G.A. MacGibbon, et al., Expression of Fos, Jun, and Krox family proteins in Alzheimer's disease, Exp. Neurol. 147 (2015) 316–332.
[215] X. Fang, et al., Vascular protective effects of KLF2 on Aβ-induced toxicity: implications for Alzheimer's disease, Brain Res. 1663 (2015) 174–183.
[216] R.K. Gopalraj, et al., Genetic association of low density lipoprotein receptor and Alzheimer's disease, Neurobiol. Aging 26 (2005) 1–7.
[217] W.J. Lukiw, Gene expression profiling in fetal, aged, and Alzheimer hippocampus: a continuum of stress-related signaling, Neurochem. Res. 29 (2004) 1287–1297.
[218] J. Hidalgo, et al., Expression of metallothionein-I, -II, and -III in Alzheimer disease and animal models of neuroinflammation, Exp. Biol. Med. 231 (2006) 1450–1458.
[219] Q. Fu, Y. Wu, RCAN1 in the inverse association between Alzheimer's disease and cancer, Oncotarget 9 (2018) 54–66.
[220] S. Saleem, S.C. Biswas, Tribbles pseudokinase 3 induces both apoptosis and autophagy in Amyloid-β-induced neuronal death, J. Biol. Chem. 292 (2017) 2571–2585.
[221] M. Chiappelli, et al., VEGF gene and phenotype relation with Alzheimer's disease and mild cognitive impairment, Rejuvenation Res. 9 (2006) 485–493.
[222] F.M. Gosso, et al., Exploring the functional role of the CHRM2 gene in human cognition: results from a dense genotyping and brain expression study, BMC Med. Genet. 8 (2007) 66.
[223] P.A. Channar, et al., Sulfonamide-Linked Ciprofloxacin, Sulfadiazine and Amantadine Derivatives as a Novel Class of Inhibitors of Jack Bean Urease; Synthesis, Kinetic Mechanism and Molecular Docking, Molecules 22 (August (8)) (2017) pii: E1352.
[224] K.J. Wu, et al., Small molecule Pin1 inhibitor blocking NF-κB signaling in prostate Cancer cells, Chem. Asian J. 13 (3) (2018) 275–279.
[225] R. Wang, et al., Comparative evaluation of 11 scoring functions for molecular docking, J. Med. Chem. 46 (12) (2003) 2287–2303.
[226] K.J. Wu, et al., 1 Structure-based identification of a NEDD8-activating enzyme inhibitor via drug repurposing, Eur. J. Med. Chem. 143 (2018) 1021–1027.
[227] O. Trott, A.J. Olson, AutoDock Vina: improving the speed and accuracy of docking with a new scoring function, efficient optimization, and multithreading, J. Comput. Chem. 31 (January (2)) (2010) 455–461.
[228] C. Yang, et al., Discovery of a VHL and HIF1α interaction inhibitor with in vivo angiogenic activity via structure-based virtual screening, Chem. Commun. (Camb.) 52 (87) (2016) 12837–12840.